DAMAGE RESPONSE OF SANDWICH PLATES SUBJECT TO DYNAMIC LOADS

by

Alfonso de Lacruz Alvarez

Naval Architect and Marine Engineer, E.T.S. Ingenieros Navales.
Madrid (Spain), 1993

Submitted to the Department of Ocean Engineering and the Department of Materials Science and Engineering in Partial Fulfillment of the Requirements for the Degrees of

MASTER OF SCIENCE IN NAVAL ARCHITECTURE AND MARINE ENGINEERING
and
MASTER OF SCIENCE IN MATERIALS SCIENCE AND ENGINEERING
at the
MASSACHUSETTS INSTITUTE OF TECHNOLOGY
June, 1995

Signature of Author_____
Department of Ocean Engineering
May 12, 1995

Certified by_____
Tomasz Wierzbicki, Professor of Applied Mechanics
Thesis Supervisor, Deparment of Ocean Engineering

Certified by_____
Frederick J. McGarry, Professor of ~~Civil Engineering and~~ Polymer Engineering
Thesis Reader, Department of Materials Science and Engineering

Accepted by _____
Carl V. Thompson II, Professor of Electronic Materials
Chairman, Materials Science and Engineering Departamental Graduate Comitee

Accepted by _____
A. Douglas Carmichael, Professor ~~of Power~~ Engineering
Chairman, Ocean Engineering Departamental Graduate Comitee

DAMAGE RESPONSE OF SANDWICH PLATES SUBJECT TO DYNAMIC LOADS

by

Alfonso de Lacruz Alvarez

Submitted to the Department of Ocean Engineering and the Department of Materials Science and Engineering on May 12, 1995 in Partial Fulfillment of the Requirements for the Degrees of Master of Science in Naval Architecture and Marine Engineering and Master of Science in Materials Science and Engineering.

ABSTRACT

The objective of this thesis is to derive closed-form solutions for the local impact response of sandwich panels. The indentation load-central deflection characteristic is obtained for three different facesheets: (1) a fully-plastic, isotropic facesheet, (2) an elastic, isotropic facesheet, and (3) an elastic, orthotropic facesheet. The honeycomb core is modeled as a rigid-plastic foundation in the formulation of the local impact response. The analysis is confined to impact situations in which the facesheet deflections are several times its thickness. This allows one to consider the face plate as a membrane on a rigid-plastic foundation since bending moments are negligible when compared to membrane forces. The problem is considered as "quasi-dynamic." The inertia of the projectile is taken into account while the inertia of the plate is ignored because the mass of the deforming facesheet is negligible compared to that of the projectile. A cornerstone of this analysis is that moving boundary conditions are applied at the extent of deformation. The analytical results are correlated to the experimental work on projectile impact into aluminum facesheets and aluminum honeycomb by W. Goldsmith and J.L. Sackman (1992), and into graphite/epoxy facesheets and nomex honeycomb by J.E. Williamson (1991). The analytical predictions for the central deflection of the plate when subjected to low velocity impact loads are within 5% error for the fully-plastic, isotropic facesheet and 10% error for the elastic, orthotropic one when the deflections are several times the thickness of the facesheets.

Thesis Supervisor: Tomasz Wierzbicki
Title: Professor of Applied Mechanics

To my parents

ACKNOWLEDGMENTS

I wish to express my gratitude to everyone who supported me during my studies at M.I.T. I am specially grateful to Dr. Michelle S. Hoo Fatt without whom I would not have been able to complete this thesis. Her guidance, patience, encouragement, and continuous support have been essential during this hard and long last semester in graduate school. I owe my gratitude to Professor Paul A. Lagace and Professor Werner Goldsmith for the experimental data used throughout this thesis.

I would also like to thank Professor Tomasz Wierzbicki. Working with him has been a privilege and a pleasure. Special thanks to my advisor at Ocean Engineering, Professor Ernst G. Frankel, and to Professor Frederick J. McGarry for their invaluable advice.

Finally, to the entire M.I.T. Community, these two years have been a worth while experience that I will never forget.

TABLE OF CONTENTS

LIST OF FIGURES

LIST OF TABLES

NOMENCLATURE

E	Young's modulus
E_L	Longitudinal stiffness
E_T	Transverse stiffness
G_{LT}	Shear modulus
σ_o	Flow stress
ν	Poisson's ratio
ρ	Density
q_z	Crushing resistance in z direction
q_{xy}, q_r	Shear transmitted by the core to the facesheet
h	Thickness of the plate
H	Thickness of the core
r_p	Radius of the impactor
σ_x	Normal stress in x direction
σ_y	Normal stress in y direction
σ_z	Normal stress in z direction
σ_r	Normal stress in radial direction
σ_θ	Normal stress in hoop direction
u_x	Displacement in x direction
u_y	Displacement in y direction
u_z	Displacement in z direction
u	Deflection of midplane ($z = h/2$) in x or radial direction
v	Deflection of midplane ($z = h/2$) in y or hoop direction
w	Deflection of midplane ($z = h/2$) in z direction
ε_x	Normal strain in x direction

ε_y	Normal strain in y direction
γ_{xy}	Shear strain
ε_{xo}	Normal strain of the midplane in x direction
ε_{yo}	Normal strain of the midplane in y direction
γ_{xyo}	Shear strain of the midplane
κ_x	Curvature in x direction
κ_y	Curvature in y direction
κ_{xy}	Twisting curvature
N_x	In-plane axial force per unit length in x direction
N_y	In-plane axial force per unit length in y direction
N_{xy}	In-plane shear force per unit length
M_x	Bending moment in x direction
M_y	Bending moment in y direction
M_{xy}	Torsional moment
Q_x, Q_y	Shear forces
u_r	Displacement in radial direction
u_θ	Displacement in hoop direction
ε_r	Normal strain in radial direction
ε_θ	Normal strain in tangential direction
$\gamma_{r\theta}$	Shear strain
ε_{ro}	Normal strain of the midplane in radial direction
$\varepsilon_{\theta o}$	Normal strain of the midplane in hoop direction
$\gamma_{r\theta o}$	Shear strain of the midplane
κ_r	Curvature in radial direction
κ_θ	Curvature in tangential direction
$\kappa_{r\theta}$	Twisting curvature
N_r	In-plane axial force per unit length in radial direction

N_θ	In-plane axial force per unit length in hoop direction
$N_{r\theta}$	In-plane shear force per unit length
M_x	Bending moment in radial direction
M_y	Bending moment in hoop direction
M_{xy}	Torsional moment
C	Extensional rigidity
D	Bending or flexural rigidity
P	Total indentation load
ξ	Extent of deformation
Π	Total potential energy
U	Internal strain energy
U_b	Internal energy due to bending moments
U_m	Internal energy due to membrane forces
W	Work due to applied external forces
E_k	Kinetic energy
M_o	Mass of the projectile
V_o	Velocity of the projectile
M_p	Mass of the facesheet under the projectile
m	Mass density of the facesheet per unit area
F_{plate}	Inertia of the facesheet
F_{proj}	Inertia of the projectile

1. INTRODUCTION

During the last three decades, sandwich structures have been steadily replacing wood, aluminum, steel and solid fiberglass in the marine industry. Initially they were only used for small crafts because their behavior was not completely understood and the shipbuilding industry was overly conservative. Today, we see them being used in structures weighing more than a hundred tonnes such as ship hulls and superstructures, and submersibles. The development has been even more prevalent in high performance applications because of the great advantages they offer over classical configurations. For example, all the high performance sailing yachts such as America's Cup boats, Whitbread 60's, or round-the-world multihulls are built using composite sandwich panels. The most common configuration for these applications is graphite/epoxy facesheets and honeycomb core. They are also extensively used in other applications such as racing powerboats and fast military crafts where good impact resistance, high stiffness-to-weight ratio, and high strength-to-weight ratio are important requirements.

Sandwich structures exhibit several advantages over conventional structures that have favored their introduction in many structural applications [1, 27, 34]: (1) they have high bending-stiffness-to-weight ratios; (2) they show good stability under compressive forces in the plane of the panel; (3) their lightweight core material acts as an energy absorber during impact events; (4) they allow more usable interior volume when compared to stiffened panels; (5) they have excellent thermal and acoustic insulation capabilities.

The idea behind a sandwich structure is the use of a low density core between two faceplates to increase the moment of inertia and, therefore, the bending stiffness of the panel without increasing the weight. In an ideal sandwich, two thin facesheets or skins are connected or bonded to two sets of ribs that run perpendicular to each other. In order for the structure to be effective, the ribs must be continuous over the length, width, and

thickness, and the cells that the ribs form must be small enough not to fail locally under lateral pressure or concentrated loads [5]. This ideal sandwich is difficult to fabricate and has been substituted for more practical configurations such as honeycomb and balsa cores. These are almost ideal except for the discontinuity of the ribs in the longitudinal and transverse directions.

The sandwich configuration is similar to an I-beam in geometry and in the way loads are transferred in it. The facesheets are like the flanges of the beam one being in tension and the other in compression when the beam is loaded. The core material acts like the web of the beam resisting compression and transverse shear loads. A structural adhesive capable of transferring shear forces from the skins to the core is used for bonding the two constituents of the sandwich.

Facesheet materials

Fiber reinforced laminates are the most common choice for the facesheets of sandwich panels in marine applications. There is a clear distinction between the composite materials used for high performance and commercial applications. Chopped, woven or unidirectional E-glass laminates are almost the only fibers used in commercial applications because they are inexpensive. On the other hand, woven and mostly unidirectional high modulus fibers such as graphite, kevlar, or boron are used in high performance structures.

Fiber reinforced laminates present some important characteristics that make them more attractive than metals for certain applications. First and foremost, they have a higher specific strength and stiffness than metals. This allows important reductions of structural weight and consequently improvements in range, speed, and payload. Second, an important characteristic is their adaptability to specific loading or structural requirements by aligning fibers in the appropriate directions. They show, in general, good fatigue characteristics and exceptional characteristics in the case of carbon or boron fibers. They present better durability and environmental resistance than metals because they are not susceptible to corrosion, rots, and marine borers. These characteristics also allow for great

reductions in maintenance costs. For commercial applications, composite materials offer a higher quality of the finished products with smooth surfaces, excellent appearance, and ease of the maintenance and repair operations. Other advantages include good toughness behavior, non-magnetic and dielectric properties, and low thermal conductivity. Despite all the advantages composite materials have to offer, uncertainty in their complex behavior and the lack of acceptance in replacing them for better understood materials have resulted in their underutilized potential.

Core materials

Three types of core materials are generally used in marine applications: wood (mainly balsa), polystyrene, polyvinyl chloride (PVC), polyurethane and acrylic foams, and aramid paper or aluminum honeycomb [31]. Balsa cores have a high compressive strength and modulus, high shear strength, and low cost, but the high resin and water absorption have made them undesirable for some marine applications. Foam cores can be divided in two groups: those with low cost and low mechanical properties such as polyurethane or polystyrene foams and those with good mechanical properties and higher cost like PVC or acrylic foams. Both types are generally used for commercial applications depending their choice on the specific mechanical requirements. Although they show excellent mechanical properties, honeycomb cores are only used for high performance applications due to their high cost. Their reduced weight and high compressive and transverse shear strengths make them the only choice for those applications even though high density PVC is also used where attachments are to be made.

Due to increasing use of sandwich structures, it is important to clearly understand their complex behavior so that they may be properly designed for particular applications. Many studies are being carried out to increase our knowledge on these configurations especially in the aircraft industry. In the marine industry, one area of major concern is the resistance of high speed vessels built of sandwich structures and subjected to impact loads [2]. There have been cases of separations of the outer facesheet from the core over a large

part of the hull due to impact loads. These loads include the collision with a rock or grounding, the collision with another vessel, or the striking of small submerged or floating objects in the water. A particular case of impact that affect the forward sections of fast crafts is that due to slamming loads. These loads are generated by the impact of waves onto hulls or by the sudden submergence of the bow into the water. Although it is not exactly a projectile impact event, it can be modeled as one by considering the loading as a uniformly distributed impulsive load over a localized or "patch" region of the plate [34, 35].

It is essential to understand the behavior of the sandwich panel during an impact event in order to prevent possible damage. There are several numerical codes for analyzing the impact response of a sandwich plate that show good correlation with experimental data until the failure of the facesheet such as those by Tsang [24] and Lie [25]. The objective of this thesis is to derive simple closed-form solutions for the impact response of sandwich panels. These solutions may be used to improve the design of sandwich hulls against impact loads.

During impact, the deformation of the bottom and side panels of the hull can be characterized by two modes: (1) overall bending of the panel and (2) local deformation of the outer facesheet and the core but no deformation of the inner facesheet. If the overall panel is assumed of infinite stiffness, only localized damage of the outer facesheet and the core will occur. The inner laminate of the sandwich remains intact and the outer one suffers permanent deformation due to plastic deformation of the core. On the other hand, for panels of overall finite stiffness, both the inner and the outer laminates undergo bending deformation.

Although the global effect should be study in order to completely understand the failure mechanisms due to impact loads, the complexity of the plate response and the damage mechanisms have limited this study to consider only the local impact response,

i.e., localized damage of the top facesheet and the core. Moreover, only low velocity impact will be considered to take advantage of the existing experimental work.

First, a general formulation of the dynamic response of a sandwich plate is given in Chapter 2. Then, three different sandwich configurations composed of three different facesheet materials and honeycomb cores are considered: a fully-plastic, isotropic facesheet in Chapter 3; an elastic, isotropic facesheet in Chapter 4; and an elastic, orthotropic facesheet in Chapter 5. The analytical results for the fully-plastic, isotropic facesheet are compared to the experimental work on projectile impact of aluminum facesheets with aluminum honeycomb core by W. Goldsmith and J.L. Sackman [15], while those for the elastic, orthotropic plate are compared to the work on projectile impact of graphite/epoxy faceplates with nomex honeycomb core by J.E. Williamson [23]. In both experimental papers, the deflections were several times the thickness of the facesheets. In those cases, the facesheets are in their membrane state.

2. PROBLEM FORMULATION

To study the local impact response of a sandwich plate, consider the top facesheet fixed onto a rigid foundation. The bottom laminate of the sandwich remains intact while the top one undergoes permanent deformation as the core crushes under the impacting force. The deformation considered is very localized so that the impact occurs over an infinite plate.

The sandwich structure is composed by two facesheets and a rigid-plastic honeycomb core. The geometry of the plate is defined by the facesheet thickness h, and honeycomb thickness H as shown in Figure 1. The faceplate is characterized by the Young's modulus E, density ρ, and Poisson's ratio ν. The projectile impact force is represented by a quasi-static punch load acting on a circular area of radius r_p. During impact, the shear transmitted by the core to the plate is denoted q_{xy}, and the crushing resistance of the honeycomb is denoted q_z.

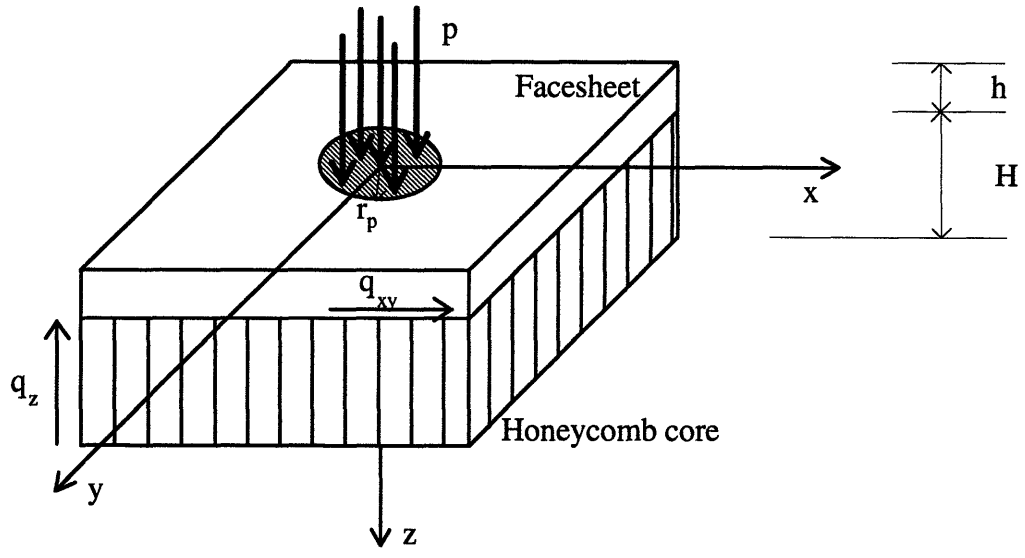

Figure 1: Geometry of the sandwich plate under the punch load.

2.1. ASSUMPTIONS

1. Since the plate is considered to be infinite, the thickness of the facesheets is small compared to the other dimensions of the plate. Therefore, the facesheets are considered thin plates and the normal stress in z direction can be neglected i.e., plane stress conditions ($\sigma_z << \sigma_x, \sigma_y \Rightarrow \sigma_z = 0$). Furthermore, due to the fact that the facesheet is thin, it is under a two dimensional state of stress ($\tau_{zx} = \tau_{zy} = 0$).

2. Plane sections remain plane and perpendicular to the midplane after deformation

$$u_x = u - z\frac{\partial w}{\partial x} \quad ; \quad u_y = v - z\frac{\partial w}{\partial y} \quad ; \quad u_z = w, \tag{1}$$

where u , v and w are the deflections of the midplane (z = h/2).

3. For a given central deflection w_o, the extent of deformation is denoted by ξ. The plate is flat and the facesheets are securely bonded to the honeycomb core. Therefore, since the displacements in x and y directions are equal to zero at x = 0 , y = 0 and at x , y larger than the extent of the deformation, they can be neglected when compared to the vertical deflection,

$$u \approx 0 \quad \text{and} \quad v \approx 0.$$

Therefore, the deflection of the plate is due to the displacement of the middle surface points in the vertical direction only.

2.2. STRAIN - DISPLACEMENT EQUATIONS

The relationships between the normal and shear strains and the displacements can be calculated using Equation (1) and taking into account that the deflections are large and the squares of the slopes are not negligible

$$\varepsilon_x = \frac{\partial u_x}{\partial x} = \varepsilon_{x_o} + z\kappa_x$$

$$\varepsilon_y = \frac{\partial u_y}{\partial y} = \varepsilon_{y_o} + z\kappa_y \tag{2}$$

$$\gamma_{xy} = \frac{\partial u_x}{\partial y} + \frac{\partial u_y}{\partial x} = \gamma_{xy_o} + z\kappa_{xy},$$

where ε_{xo}, ε_{yo}, and ε_{xyo} are the strains of the neutral surface, and κ_x, κ_y, and κ_{xy} are the curvatures. The strains of the midplane and the curvatures are defined as

$$\varepsilon_{x_o} = \frac{\partial u}{\partial x} + \frac{1}{2}\left(\frac{\partial w}{\partial x}\right)^2$$

$$\varepsilon_{y_o} = \frac{\partial v}{\partial y} + \frac{1}{2}\left(\frac{\partial w}{\partial y}\right)^2 \tag{3}$$

$$\gamma_{xy_o} = \left(\frac{\partial u}{\partial y} + \frac{\partial v}{\partial x}\right) + \frac{\partial w}{\partial x}\frac{\partial w}{\partial y},$$

and

$$\kappa_x = -\frac{\partial^2 w}{\partial x^2}$$

$$\kappa_y = -\frac{\partial^2 w}{\partial y^2} \tag{4}$$

$$\kappa_{xy} = -2\frac{\partial^2 w}{\partial x \partial y}.$$

2.3. EQUILIBRIUM OF FORCES AND MOMENTS

The stresses in the plate are written in terms of the strains using Hooke's law

$$\sigma_x = \frac{E}{1-\nu^2}\left(\varepsilon_x + \nu\varepsilon_y\right)$$

$$\sigma_y = \frac{E}{1-\nu^2}\left(\varepsilon_y + \nu\varepsilon_x\right) \tag{5}$$

$$\tau_{xy} = \frac{E}{2(1+\nu)}\gamma_{xy}.$$

Once the relationship between stresses and strains has been established, the in-plane forces per unit length are calculated as the integral of the stresses over the thickness of the plate

$$N_x = \int_{-h/2}^{h/2} \sigma_x dz = C\left(\varepsilon_{x_o} + \nu\varepsilon_{y_o}\right)$$

$$N_y = \int_{-h/2}^{h/2} \sigma_y dz = C\left(\varepsilon_{y_o} + \nu\varepsilon_{x_o}\right) \tag{6}$$

$$N_{xy} = \int_{-h/2}^{h/2} \tau_{xy} dz = C \frac{(1-\nu)}{2} \gamma_{xy_o},$$

where $C = \frac{Eh}{1-\nu^2}$ is the extensional rigidity.

The relationship between membrane forces and displacements is derived by introducing Equations (3) into Equations (6)

$$N_x = C\left(\frac{\partial u}{\partial x} + \frac{1}{2}\left(\frac{\partial w}{\partial x}\right)^2 + \nu \frac{\partial v}{\partial y} + \frac{\nu}{2}\left(\frac{\partial w}{\partial y}\right)^2\right)$$

$$N_y = C\left(\frac{\partial v}{\partial y} + \frac{1}{2}\left(\frac{\partial w}{\partial y}\right)^2 + \nu \frac{\partial u}{\partial x} + \frac{\nu}{2}\left(\frac{\partial w}{\partial x}\right)^2\right) \tag{7}$$

$$N_{xy} = C \frac{(1-\nu)}{2}\left(\left(\frac{\partial u}{\partial y} + \frac{\partial v}{\partial x}\right) + \frac{\partial w}{\partial x}\frac{\partial w}{\partial y}\right).$$

Bending moments are also calculated from the stress-strain relationships by integration of stresses and moment arms

$$M_x = \int_{-h/2}^{h/2} \sigma_x z dz = D(\kappa_x + \nu\kappa_y)$$

$$M_y = \int_{-h/2}^{h/2} \sigma_y z dz = D(\kappa_y + \nu\kappa_x) \tag{8}$$

$$M_{xy} = \int_{-h/2}^{h/2} \tau_{xy} z dz = D(1-\nu)\kappa_{xy},$$

where $D = \dfrac{Eh^3}{12(1-\nu^2)}$ is the bending or flexural rigidity.

Equilibrium of the facesheet gives

$$\frac{\partial N_x}{\partial x} + \frac{\partial N_{yx}}{\partial y} = q_{xy} + h\rho \frac{\partial^2 u}{\partial t^2} \tag{9}$$

in x-direction,

$$\frac{\partial N_{xy}}{\partial x} + \frac{\partial N_y}{\partial y} = q_{yx} + h\rho \frac{\partial^2 v}{\partial t^2} \tag{10}$$

in y-direction, and

$$\frac{\partial Q_x}{\partial x} + \frac{\partial Q_y}{\partial y} + N_x \frac{\partial^2 w}{\partial x^2} + 2N_{xy} \frac{\partial^2 w}{\partial x \partial y} + N_y \frac{\partial^2 w}{\partial y^2} + \frac{\partial w}{\partial x}\left(\frac{\partial N_x}{\partial x} + \frac{\partial N_{yx}}{\partial y}\right) + \frac{\partial w}{\partial y}\left(\frac{\partial N_{xy}}{\partial x} + \frac{\partial N_y}{\partial y}\right) +$$

$$+(p - q_z) = \rho h \frac{\partial^2 w}{\partial t^2} \tag{11}$$

in z-direction.

On the other hand, moment equilibrium gives

$$\frac{\partial M_x}{\partial x} + \frac{\partial M_{xy}}{\partial x} = Q_x \tag{12}$$

in x-direction, and

$$\frac{\partial M_{xy}}{\partial x} + \frac{\partial M_y}{\partial x} = Q_y \tag{13}$$

in y-direction, where Q_x and Q_y are shear forces.

2.4. GOVERNING EQUATIONS OF MOTION

The combination of the equilibrium equations in the three directions, Equations (9), (10) and (11), gives

$$\frac{\partial Q_x}{\partial x} + \frac{\partial Q_y}{\partial y} + N_x \frac{\partial^2 w}{\partial x^2} + 2N_{xy} \frac{\partial w}{\partial x \partial y} + N_y \frac{\partial^2 w}{\partial y^2} +$$

$$+ \frac{\partial w}{\partial x}\left(q_{xy} + h\rho \frac{\partial^2 u}{\partial t^2}\right) + \frac{\partial w}{\partial y}\left(q_{yx} + h\rho \frac{\partial^2 v}{\partial t^2}\right) + (p - q_z) = h\rho \frac{\partial^2 w}{\partial t^2}. \tag{14}$$

If moment equilibrium equations, Equations (12) and (13), are introduced into Equation (14),

$$\frac{\partial^2 M_x}{\partial x^2} + 2\frac{\partial^2 M_{xy}}{\partial x \partial y} + \frac{\partial^2 M_y}{\partial y^2} + N_x \frac{\partial^2 w}{\partial x^2} + 2N_{xy} \frac{\partial w}{\partial x \partial y} + N_y \frac{\partial^2 w}{\partial y^2} +$$

$$+ \frac{\partial w}{\partial x}\left(q_{xy} + h\rho \frac{\partial^2 u}{\partial t^2}\right) + \frac{\partial w}{\partial y}\left(q_{yx} + h\rho \frac{\partial^2 v}{\partial t^2}\right) + (p - q_z) = h\rho \frac{\partial^2 w}{\partial t^2}. \tag{15}$$

Equations (4) are introduced into Equations (8) to get an explicit relationship between bending moments and displacements

$$M_x = D(\kappa_x + \nu\kappa_y) = -D\left(\frac{\partial^2 w}{\partial x^2} + \nu\frac{\partial^2 w}{\partial y^2}\right)$$

$$M_y = D(\kappa_y + \nu\kappa_x) = -D\left(\frac{\partial^2 w}{\partial y^2} + \nu\frac{\partial^2 w}{\partial x^2}\right) \qquad (16)$$

$$M_{xy} = D(1-\nu)\kappa_{xy} = -D(1-\nu)\frac{\partial^2 w}{\partial x \partial y}.$$

Substituting, Equations (16), into Equation (15) gives

$$-D\left(\frac{\partial^4 w}{\partial x^4} + 2\frac{\partial^4 w}{\partial x^2 \partial y^2} + \frac{\partial^4 w}{\partial y^4}\right) + N_x\frac{\partial^2 w}{\partial x^2} + 2N_{xy}\frac{\partial w}{\partial x \partial y} + N_y\frac{\partial^2 w}{\partial y^2} +$$

$$+\frac{\partial w}{\partial x}\left(q_{xy} + h\rho\frac{\partial^2 u}{\partial t^2}\right) + \frac{\partial w}{\partial y}\left(q_{yx} + h\rho\frac{\partial^2 v}{\partial t^2}\right) + (p - q_z) = h\rho\frac{\partial^2 w}{\partial t^2}, \qquad (17)$$

or

$$D\nabla^4 w - N_x\frac{\partial^2 w}{\partial x^2} - 2N_{xy}\frac{\partial w}{\partial x \partial y} - N_y\frac{\partial^2 w}{\partial y^2} - \frac{\partial w}{\partial x}\left(q_{xy} + h\rho\frac{\partial^2 u}{\partial t^2}\right) -$$

$$-\frac{\partial w}{\partial y}\left(q_{yx} + h\rho\frac{\partial^2 v}{\partial t^2}\right) = (p - q_z) - h\rho\frac{\partial^2 w}{\partial t^2}. \qquad (18)$$

where $\nabla = \frac{\partial}{\partial x^2} + \frac{\partial}{\partial y^2}$ is the Laplacian operator.

2.5. SUMMARY OF PLATE EQUILIBRIUM EQUATIONS

The equilibrium equations of the plate under the quasi-static punch load are:

- $$\frac{\partial N_x}{\partial x} + \frac{\partial N_{yx}}{\partial y} = q_{xy} + h\rho \frac{\partial^2 u}{\partial t^2} \tag{9}$$

- $$\frac{\partial N_{xy}}{\partial x} + \frac{\partial N_y}{\partial y} = q_{yx} + h\rho \frac{\partial^2 v}{\partial t^2} \tag{10}$$

- $$D\nabla^4 w - N_x \frac{\partial^2 w}{\partial x^2} - 2N_{xy} \frac{\partial w}{\partial x \partial y} - N_y \frac{\partial^2 w}{\partial y^2} - \frac{\partial w}{\partial x}\left(q_{xy} + h\rho \frac{\partial^2 u}{\partial t^2}\right) -$$

$$- \frac{\partial w}{\partial y}\left(q_{yx} + h\rho \frac{\partial^2 v}{\partial t^2}\right) = (p - q_z) - h\rho \frac{\partial^2 w}{\partial t^2} \tag{18}$$

The above expression, Equation (18), is the governing equation for the plate vertical deflection including both membrane forces and bending moments.

2.6. SIMPLIFICATIONS

1. When the deflections of the plate are large compared to the thickness as in the experimental work by Goldsmith and Sackman [15] and Williamson [23], plate bending resistance is negligible when compared to membrane one (D = 0). However, the resulting differential equation remains non-linear and can not be integrated directly. In order to estimate the value of the deflection, three cases that can be applied to different materials used in the marine industry will be considered: a fully-plastic, isotropic plate over a rigid-

plastic foundation, an elastic, isotropic plate over a rigid-plastic foundation, and an elastic, orthotropic plate over a rigid-plastic foundation.

2. The impact response of the sandwich plate is considered to be a "quasi-dynamic" process [10]. The inertia of the facesheet is neglected compared to the inertia of the projectile because the mass of the projectile is much larger than the mass of the deforming top plate.

2.7. MOVING BOUNDARY CONDITIONS

Since a local impact event is considered, the plate is bounded at infinity. However, deformations occur within a finite region ξ, as shown in Figure 2, that depends on the load intensity. Boundary conditions or, in this case, moving boundary conditions, are applied at ξ, i.e., the extent of deformation. These are:

1. The vertical deflection is zero at the extent of deformation,

$$w = 0 \quad \text{at } r = \xi, \tag{19}$$

where $r^2 = x^2 + y^2$.

2. The condition of kinematic continuity has to be satisfied at the moving boundary ξ,

$$\left[\frac{\partial w}{\partial t}\right] + \frac{\partial \xi}{\partial t}\left[\frac{\partial w}{\partial r}\right] = 0 \quad \text{at } r = \xi, \tag{20}$$

where [ ] symbolizes a jump in value across the moving boundary.

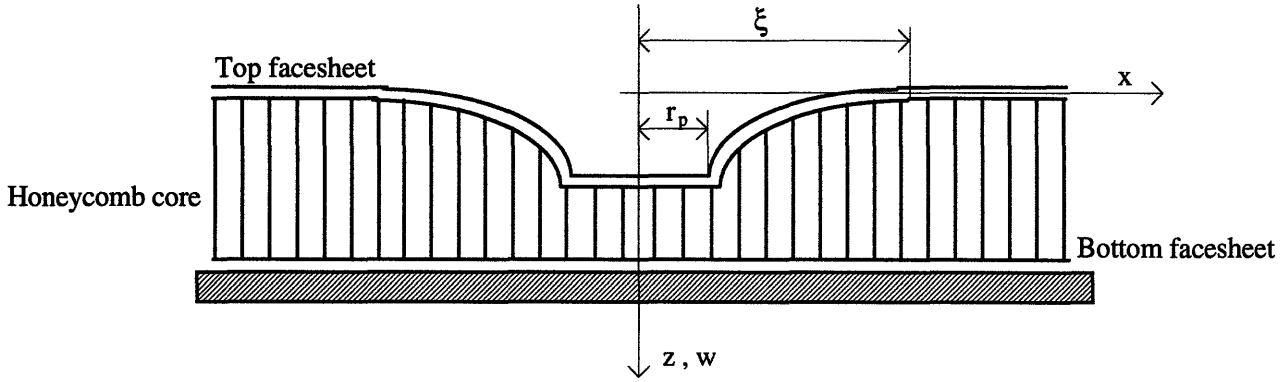

Figure 2: Cross-section of the sandwich plate through y = 0.

3. FULLY-PLASTIC, ISOTROPIC FACESHEET OVER A RIGID-PLASTIC FOUNDATION

The sandwich structure is composed by two fully-plastic, homogeneous, and isotropic facesheets and a rigid-plastic honeycomb core. The plate is considered to have infinite radius, facesheet thickness h, and honeycomb thickness H as shown in Figure 3. The facesheet is characterized by the Young's modulus E, flow stress σ_o, and Poisson's ratio ν. During deformation, the shear transferred by the core to the plate is denoted q_r, and the crushing resistance of the honeycomb is denoted q_z.

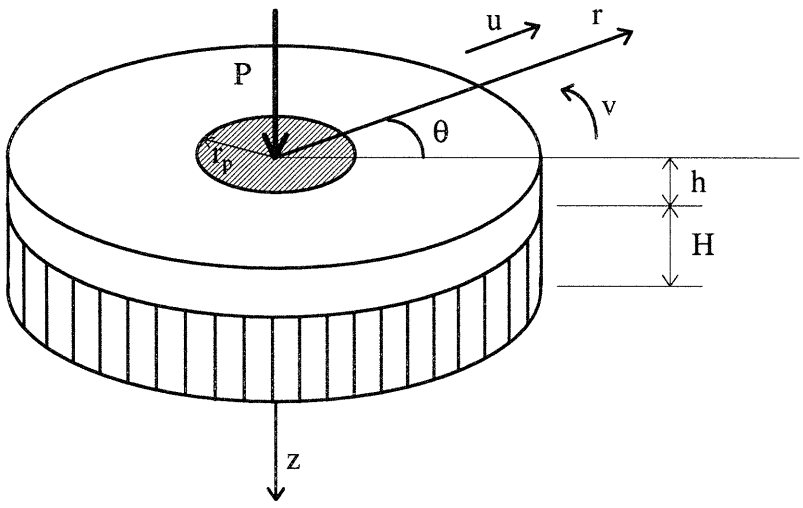

Figure 3: Geometry of the sandwich plate under the punch in polar coordinates.

The problem to be solved is that of the local effect of a quasi-static punch load acting at the center of a circular sandwich plate when the deflections are large compared to the thickness of the facesheets. The plate equations will be reformulated in polar coordinates to take advantage of the axial symmetry of the problem, i.e., there is no dependence on the hoop coordinate θ and the derivation is reduced to one dimension

$$\frac{\partial}{\partial\theta} = 0 \quad \text{and} \quad v \approx 0, \tag{21}$$

where v is the displacement in the hoop direction.

For a given central deflection w_o, the extent of deformation is denoted by ξ. The plate is flat and the facesheets are securely bonded to the honeycomb core. Therefore, since the radial displacement u is equal to zero at r smaller than r_p and at r larger than the extend of the deformation, it can be neglected when compared to the vertical deflection everywhere in the plate ($u \approx 0$).

3.1. STRAIN - DISPLACEMENT EQUATIONS

The relationships between the normal and shear strains and the displacements in polar coordinates are calculated by transforming the relationships in rectangular coordinates to polar coordinates

$$\begin{aligned} \varepsilon_r &= \varepsilon_{r_o} + z\kappa_r \\ \varepsilon_\theta &= \varepsilon_{\theta_o} + z\kappa_\theta \\ \gamma_{r\theta} &= \gamma_{r\theta_o} + z\kappa_{r\theta}, \end{aligned} \tag{22}$$

where ε_{ro}, $\varepsilon_{\theta o}$ and $\varepsilon_{r\theta o}$ are the strains of the neutral surface, and κ_r, κ_θ, and $\kappa_{r\theta}$ are the curvatures. The strains of the midplane and the curvatures are defined as

$$\varepsilon_{r_o} = \frac{\partial u}{\partial r} + \frac{1}{2}\left(\frac{\partial w}{\partial r}\right)^2 = \frac{1}{2}\left(\frac{\partial w}{\partial r}\right)^2$$

$$\varepsilon_{\theta_o} = \frac{1}{r}\frac{\partial v}{\partial \theta} + \frac{u}{r} \approx 0 \tag{23}$$

$$\gamma_{r\theta_o} = \frac{1}{r}\frac{\partial u}{\partial \theta} + \frac{\partial v}{\partial r} - \frac{v}{r} \approx 0$$

and

$$\kappa_r = -\frac{\partial^2 w}{\partial r^2}$$

$$\kappa_\theta = -\frac{1}{r}\frac{\partial w}{\partial r} - \frac{1}{r^2}\frac{\partial^2 w}{\partial \theta^2} = -\frac{1}{r}\frac{\partial w}{\partial r} \tag{24}$$

$$\kappa_{r\theta} = -\frac{2}{r}\frac{\partial^2 w}{\partial r \partial \theta} + \frac{2}{r^2}\frac{\partial w}{\partial \theta} = 0.$$

3.2. STRESS - STRAIN EQUATIONS

In-plane forces per unit length are calculated using Hooke's law to formulate the relationships between stresses and strains and a transformation of reference system to polar coordinates

$$N_r = C\left(\varepsilon_{r_o} + \nu\varepsilon_{\theta_o}\right)$$

$$N_\theta = C\left(\varepsilon_{\theta_o} + \nu\varepsilon_{r_o}\right) \tag{25}$$

$$N_{r\theta} = C\frac{(1-\nu)}{2}\gamma_{r\theta_o},$$

where $C = \dfrac{Eh}{1-\nu^2}$ is the extensional rigidity.

Membrane forces are expressed in terms of the vertical displacement of the plate by introducing Equations (23) into Equations (25)

$$N_r = \frac{C}{2}\left(\frac{\partial w}{\partial r}\right)^2 \tag{26}$$

$$N_\theta = \frac{C\nu}{2}\left(\frac{\partial w}{\partial r}\right)^2 \tag{27}$$

$$N_{r\theta} = 0. \tag{28}$$

Bending moments are derived in the same way as in the rectangular coordinate system formulation but transforming the coordinate system to polar

$$\begin{aligned} M_r &= D(\kappa_r + \nu\kappa_\theta) \\ M_\theta &= D(\kappa_\theta + \nu\kappa_r) \\ M_{r\theta} &= D\left(\frac{1-\nu}{2}\right)\kappa_{r\theta}, \end{aligned} \tag{29}$$

where $D = \dfrac{Eh^3}{12(1-\nu^2)}$ is the bending or flexural rigidity.

Equations (24) are introduced into Equations (29) to derive an explicit relationship between bending moments and the vertical displacement

$$M_r = -D\left(\frac{\partial^2 w}{\partial r^2} + \frac{\nu}{r}\frac{\partial w}{\partial r}\right) \tag{30}$$

$$M_\theta = -D\left(\frac{1}{r}\frac{\partial w}{\partial r} + \nu\frac{\partial^2 w}{\partial r^2}\right) \tag{31}$$

$$M_{r\theta} = 0. \tag{32}$$

3.3. EQUILIBRIUM OF FORCES AND MOMENTS

The equilibrium of forces acting in radial direction gives

$$r\frac{\partial N_r}{\partial r} + (N_r - N_\theta) - q_r = 0. \tag{33}$$

Furthermore, since the displacement of the plate is only in vertical direction (u , v ≈ 0), the shear transmitted by the core to the plate is zero ($q_r = 0$). The resulting equilibrium equation in radial direction is

$$r\frac{\partial N_r}{\partial r} + (N_r - N_\theta) = 0. \tag{34}$$

The moment equilibrium equation of the facesheet can be written as

$$\frac{\partial}{\partial r}\left(r\frac{\partial M_r}{\partial r} + M_r - M_\theta - rN_r\frac{\partial w}{\partial r}\right) = q_z r. \tag{35}$$

Equation (35) is expressed in terms of the vertical displacement of the plate by introducing Equations (30) and (31)

$$\frac{\partial}{\partial r}\left[-Dr\left(\frac{\partial^3 w}{\partial r^3} + \frac{1}{r}\frac{\partial^2 w}{\partial r^2} - \frac{1}{r^2}\frac{\partial w}{\partial r}\right) + rN_r\frac{\partial w}{\partial r}\right] = q_z r. \tag{36}$$

Equation (36) is the governing differential equation for the vertical deflection of the facesheet in polar coordinates that includes not only membrane forces but also bending moments.

In the experiments conducted by Goldsmith and Sackman [15] that will be used to validate the analytical results for the fully-plastic, isotropic plate, the deflections are several times the thickness of the facesheet. Being under large deflection conditions, bending moments can be neglected when compared to membrane forces (D = 0) and Equation (36) simplifies into

$$\frac{\partial}{\partial r}\left(rN_r \frac{\partial w}{\partial r}\right) = q_z r. \tag{37}$$

3.4. BOUNDARY CONDITIONS

This governing equation for the facesheet vertical deflection is subjected to the following boundary conditions:

1. When subjected to large deflections, the total shear force of the plate is equal to the total indentation force P plus the crushing resistance of the honeycomb under the punch

$$N_r \frac{\partial w}{\partial r}\left(2\pi r_p\right) = -\left(P - q_z \pi r_p^{\,2}\right) \quad \text{at r} = \text{r}_\text{p}. \tag{38}$$

2. The vertical deflection is zero at the extent of deformation

$$w = 0 \quad \text{at } r = \xi \tag{39}$$

as shown in Figure 4.

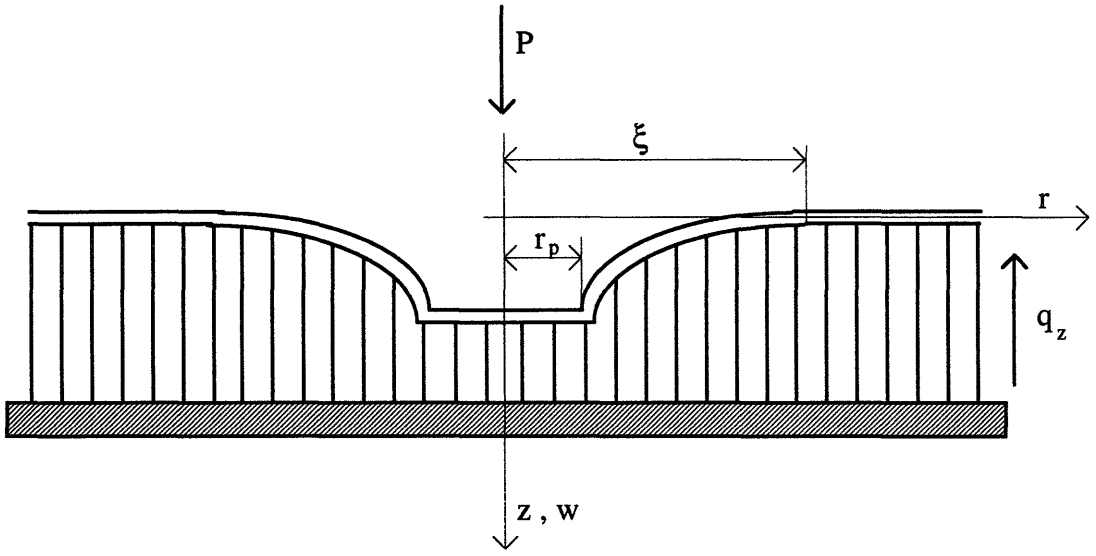

Figure 4: Cross-section of the sandwich plate.

Because the extent of deformation or boundary between the deformed and non-deformed regions changes during the loading process, the condition of kinematic continuity of the vertical deflection must be also satisfied at ξ,

$$\left[\frac{\partial w}{\partial t}\right] + \frac{\partial \xi}{\partial t}\left[\frac{\partial w}{\partial r}\right] = 0 \quad \text{at } r = \xi, \tag{40}$$

where [ ] symbolizes a jump across the moving boundary. Since for r greater than ξ

$$\frac{\partial w}{\partial r} = 0 \quad \text{and} \quad \frac{\partial w}{\partial t} = 0,$$

Equation (40) can be modify to give

$$\frac{\partial w}{\partial t} + \frac{\partial \xi}{\partial t}\frac{\partial w}{\partial r} = 0 \quad \text{at r} = \xi\,. \tag{41}$$

3.5. SOLUTION

The governing differential equation for the vertical deflection of the facesheet is

$$\frac{\partial}{\partial r}\left(rN_r \frac{\partial w}{\partial r}\right) = q_z r. \tag{37}$$

Integrating Equation (37) with respect to the radial coordinate r gives

$$N_r \frac{\partial w}{\partial r} = \frac{q_z r}{2} + \frac{C_1}{r}. \tag{42}$$

The integration constant C_1 is calculated from this expression, Equation (42) using the first boundary condition

$$C_1 = -\frac{P}{2\pi}. \tag{43}$$

Since the plate is considered as fully-plastic and isotropic, the radial membrane force reaches full yield when

$$N_r = N_o = \sigma_o h. \tag{44}$$

Equation (42) can be rewritten using this fully-plastic membrane force as

$$N_o \frac{\partial w}{\partial r} = \frac{q_z r}{2} - \frac{P}{2\pi r}. \tag{45}$$

Integrating Equation (45) with respect to the radial coordinate r gives

$$N_o w = \frac{q_z r^2}{4} - \frac{P}{2\pi} \ln r + C_2. \tag{46}$$

The integration constant C_2 can be calculated using the second boundary condition (w = 0 at r = ξ) and Equation (46)

$$C_2 = \frac{P}{2\pi} \ln \xi - \frac{q_z \xi^2}{4}. \tag{47}$$

If the value of C_2 is introduced in Equation (46),

$$N_o w = \frac{P}{2\pi} \ln \frac{\xi}{r} - \frac{q_z}{4}(\xi^2 - r^2), \tag{48}$$

where ξ is function of the total indentation force P.

This relation between the extent of deformation and the total indentation load can be calculated using the condition of kinematic continuity of the vertical deflection at the moving boundary. In a quasi-static problem, the monotonically increasing load can be considered a time-like parameter and used to substitute the time in Equation (41)

$$\frac{\partial w}{\partial P} + \frac{\partial \xi}{\partial P}\frac{\partial w}{\partial r} = 0 \quad \text{at } r = \xi. \tag{49}$$

The relationship between ξ and P is obtained applying this condition to Equation (48)

$$P = \pi q_z \xi^2. \tag{50}$$

The central deflection of the plate is calculated for $r = r_p$ as a function of the extent of deformation from Equation (48) and the previous relationship between P and ξ

$$N_o w_o = \frac{q\xi^2}{2} \ln \frac{\xi}{r_p} - \frac{q_z}{4}\left(\xi^2 - r_p^{\,2}\right). \tag{51}$$

This relationship between w_o and ξ can be non-dimensionalized by introducing the following dimensionless variables:

$$\bar{\xi} = \frac{\xi}{r_p} \quad \text{and} \quad \overline{w_o} = \frac{4 N_o w_o}{q_z r_p^2}. \tag{52}$$

The present solution for the vertical deflection of the facesheet given by Equation (51) can be rewritten in terms of these new defined dimensionless variables as

$$\overline{w_o} = \overline{\xi}^2 \ln \overline{\xi}^2 - \overline{\xi}^2 + 1. \tag{53}$$

This relationship between the dimensionless extent of deformation and the dimensionless central deflection, Equation (53), can be approximated by a parabolic function with an appropriate coefficient that is calculated via minimization of the relative error

$$\left(\overline{w_o}\right)_{app} = 2.8\left(\overline{\xi} - 1\right)^2. \tag{54}$$

Both the exact solution and the parabolic approximation are shown in Figure 5.

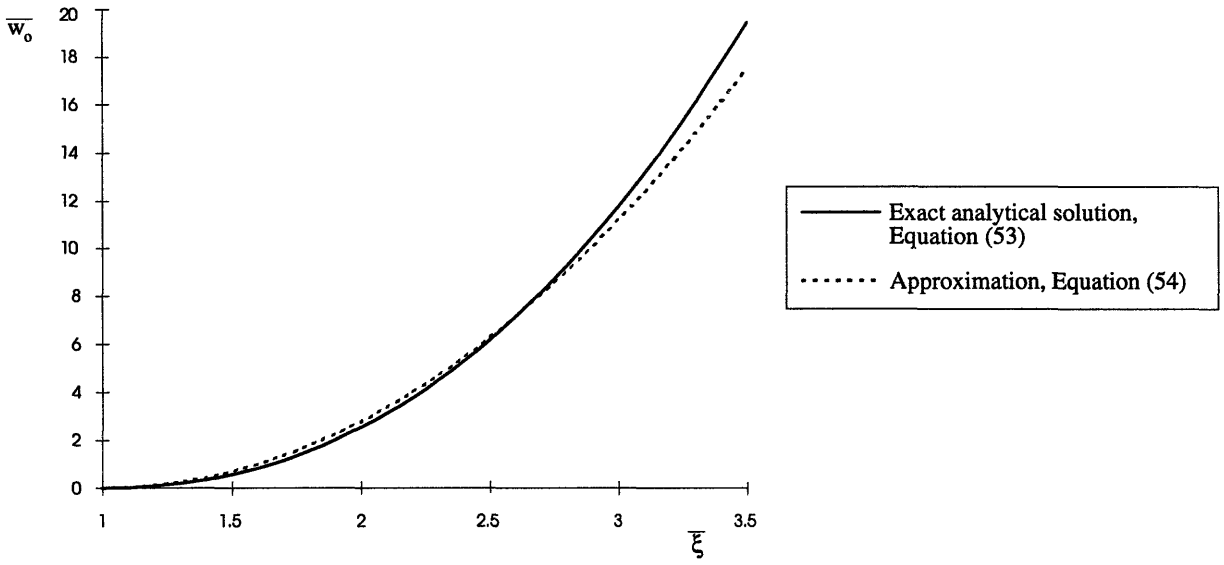

Figure 5: Exact and approximate relations between the dimensionless central deflection and the dimensionless extent of deformation for a sandwich configuration composed of a fully-plastic, isotropic facesheet and honeycomb core.

3.5.1. Introduction of impact parameters

If the impacting object is considered as a rigid cylinder of mass M_o and initial velocity V_o, the total indentation force or contact P that acts over the facesheet of the sandwich is equal to the inertia force of the projectile

$$P = -M_o \frac{\partial^2 w}{\partial t^2}. \tag{55}$$

The equations of the quasi-static approximation are still valid if the plate inertia force can be neglected compared to the inertia of the projectile. Therefore, if F_{plate} is the inertia of the facesheet and F_{proj} is the inertia of the projectile,

$$\frac{F_{plate}}{F_{proj}} << 1. \tag{56}$$

The inertia force of the top face can be calculated as the integral of the mass of the plate times the vertical acceleration

$$F_{plate} = \int_0^{\xi} 2\pi r m \frac{\partial^2 w(r)}{\partial t^2} dr = 2\pi m \int_0^{\xi} r \frac{\partial^2 w(r)}{\partial t^2} dr, \tag{57}$$

where m is the mass density of facesheet per unit area. Since the acceleration is maximum at $r = r_p$ and decreases as the radius increases, the upper bound of the inertia force of the plate would be

$$F_{plate} \leq 2\pi m \int_0^{\xi} r \frac{\partial^2 w_o}{\partial t^2} dr = \pi \xi^2 m \frac{\partial^2 w_o}{\partial t^2}. \tag{58}$$

Once the inertia of the projectile given by Equation (55) and the inertia of the facesheet given by Equation (58) are known, the relation between them can be established as

$$\frac{F_{plate}}{F_{proj}} \leq \frac{\pi r_p^2 m}{M_o} \left(\frac{\xi}{r_p} \right)^2 = \frac{M_p}{M_o} \left(\frac{\xi}{r_p} \right)^2, \tag{59}$$

where M_p denotes the mass of the facesheet under the projectile. In the above relationship and for the experimental values that Goldsmith and Sackman used in their tests, the relation ξ / r_p varies from 1 to a maximum value of 3.5, and the mass of the projectile under the punch takes a value of $M_p = 0.01M_o$. The ratio between the inertia of the plate and the inertia of the projectile varies from 0.01 to 0.035. This result validates the assumption that considered the inertia of the plate negligible when compared to the inertia of the projectile. Therefore, the equations derived under quasi-static assumptions will stil be useful to estimate the extent of deformation and the final central deflection in terms of the experimental parameters.

An energy balance between the kinetic energy transmitted by the projectile to the facesheet and the plastic work required to plastically deform the plate and crush the honeycomb can be established to relate the extent of deformation and the central deflection with the experimental parameters (M_o, V_o, σ_o, q_z, r_p and h). The kinetic energy that the projectile transmits to the plate is function of its mass and initial speed

$$E_k = \frac{1}{2} M_o V_o^2. \tag{60}$$

On the other hand, the plastic work on the sandwich plate includes the energy required to crush the honeycomb plus the energy required to plastically deform the facesheet. It is calculated from the total indentation force

$$E_{plastic} = \int_0^{w_o} P(w_o)dw_o = \int_{r_p}^{\xi} P(\xi)\frac{\partial w_o}{\partial \xi}d\xi, \tag{61}$$

where $\partial w_o / \partial \xi$ can be calculated from Equation (48) and $P(\xi)$ is known from Equation (50). The result of the integral is

$$E_{plastic} = \frac{\pi q_z^2 r_p^4}{4\sigma_o h}\left[\left(\frac{\xi}{r_p}\right)^4\left[\ln\left(\frac{\xi}{r_p}\right)^4 - 1\right] + 1\right]. \tag{62}$$

Finally, the relationship between the extent of deformation and the experimental parameters is obtained balancing both the kinetic energy communicated to the facesheet by the projectile and the plastic work required to deform the sandwich

$$E_k = \frac{1}{2}M_o V_o^2 = \frac{\pi q_z^2 r_p^4}{16\sigma_o h}\left[\left(\frac{\xi}{r_p}\right)^4\left[\ln\left(\frac{\xi}{r_p}\right)^4 - 1\right] + 1\right] = E_{plastic}. \tag{63}$$

Equation (63) can be rewritten in a non-dimensional form by using the dimensionless variables given by Equation (52)

$$\overline{E_k} = \bar{\xi}^4\left[\ln \bar{\xi}^4 - 1\right] + 1, \tag{64}$$

where the dimensionless kinetic energy is defined as

$$\overline{E_k} = \frac{8 M_o V_o^2 \sigma_o h}{\pi q_z^{\,2} r_p^4}. \tag{65}$$

Equation (64) in conjunction with Equation (53) allows the calculation of the vertical deflection of the facesheet by a previous evaluation of the extent of deformation as a function of the experimental parameters (M_o, V_o, σ_o, q_z, r_p and h). Once the extent of deformation is known, the total indentation force P can also be calculated.

3.6. DESCRIPTION OF THE EXPERIMENTAL WORK

The present analysis will be validated using the experimental work by W. Goldsmith and J.L. Sackman [15] on the impact of a flat-nosed cylindrical impactor on both bare honeycomb and sandwich plates with aluminum facesheets and aluminum honeycomb. In both cases the targets were supported by a rigid foundation while the sandwich plate was also tested under simply-supported conditions.

The tests were subjected to the following conditions: the impacting area was smaller than the lateral extent of the samples, the thickness of the core was limited to 19 mm., the diameter of the impactor was greater than cell dimensions and plate thickness, and impact velocities ranged from 10 to 40 m/s in order to just attain densification of the targets.

The present solution will be also be compared to a numerical approximation by M. Jamjian, J.L. Sackman and W. Goldsmith [12]. In their paper, the response of a thin infinite plate over a honeycomb foundation impacted by a cylindrical impactor was analyzed. The facesheet was considered as rigid-perfectly-plastic and the honeycomb as a continuum with discontinuous density. Bending moments, membrane forces and transverse

shear forces were retained in the derivation. Seven tests with different experimental parameters were chosen from the ones performed by Goldsmith and Sackman [15] and used to correlate the numerical solution. The material used was an 5052 H32 aluminum facesheet and 5052 aluminum honeycomb. The tests were performed with samples of different facesheet thicknesses and core types. The radius of the impactor used was 36.56 mm. The experimental matrix can be seen in Table 1.

Test no.	Hexcel core type	Plate thickness (mm)
1	1/4-5052-0.001	0.8128
2	1/4-5052-0.01	1.27
3	1/8-5052-0.001	1.27
4	1/8-5052-0.002	0.8128
5	1/8-5052-0.002	1.27
6	1/8-5052-0.001	1.27
7	1/8-5052-0.001	1.27

Table 1: Test matrix selected for Jamjian et al. (1994) to compare their numerical predictions for the central deflection and extent of deformation to the experimental results on the impact response of aluminum facesheets and aluminum honeycombs by Goldsmith and Sackman (1992).

3.7. RESULTS

The derived analytical equations will be correlated against the experimental results on low velocity impact by Goldsmith and Sackman [15] and the numerical predictions by Jamjian et al. [12]. The input data, the experimental results, the predictions by Jamjian et al. and the analytical solutions obtained in the present study for each of tests chosen by

Jamjian et al. to validate their approach are presented in Table 2. The relative errors for both the numerical approximation by Jamjian et al. and the present analytical result when compared to the experimental data are also included.

		Test #1	Test #2	Test #3	Test #4	Test #5	Test #6	Test #7
h	**[mm]**	0.8128	1.27	1.27	0.8128	1.27	1.27	1.27
q_r	**[N/m²]**	668795	668795	1889175	5722684	5722684	1889175	1889175
V_0	**[m/s]**	19.35	19.28	24.21	34.01	34.21	26.47	28.27
ξ [cm]	Experimental, Goldsmith & Sackman (1992)	9.14	10.54	7.23	4.83	5.27	7.74	7.87
	Jamjian et al (1994)	8.76	9.59	7.21	5.08	5.56	7.38	7.5
	Error	4.16%	9.01%	0.28%	5.18%	5.50%	4.65%	4.70%
	Present	9.57	10.4	7.74	5.71	6.09	7.99	8.17
	Error	4.69%	1.37%	7.11%	18.29%	15.51%	3.17%	3.82%
w_0 [cm]	Experimental, Goldsmith & Sackman (1992)	1.23	1.06	0.93	1.25	1.14	1.08	1.22
	Jamjian et al (1994)	1.35	1.16	1.05	1.16	1.03	1.2	1.32
	Error	9.76%	9.43%	12.90%	7.20%	9.65%	11.11%	8.20%
	Present	1.22	1.04	0.98	1.05	0.96	1.11	1.21
	Error	0.98%	1.56%	4.86%	16.10%	15.91%	2.40%	0.60%

$r_p = 3.66$ cm $\qquad \sigma_0 = 1.65 \cdot 10^8$ N/m² $\qquad M_0 = 0.839$ Kg

Table 2: Comparison of present analytical solutions for the central deflection and extent of deformation to the experimental results of Goldsmith and Sackman (1992) and the numerical predictions of Jamjian et al. (1994).

It can be seen from Table 2 that the present analytical predictions are within 5% error for low impact velocities when compared to the experimental results. Only the tests #4 and #5 with the highest impact velocities are out of the 5% error range but closer to 16% error. On the other hand, for the extent of deformation, the analytical results are within 8% error when correlated to the experimental data except for the two tests with the

highest impact velocities for which the error reaches 19%. A reasonable explanation for this increment in the error is that the problem was considered "quasi-dynamic" and the inertia of the plate was neglected. As the impactor velocity increases, the relative importance of the inertia of the facesheet also increases. It is also noticeable that the error achieved using these simple closed-form solutions is lower than that obtained by Jamjian et al. using a numerical approximation. This fact can be also observed in Figure 6 where the present analytical solutions are compared to the experimental results by Goldsmith and Sackman and the numerical approximation by Jamjian et al.

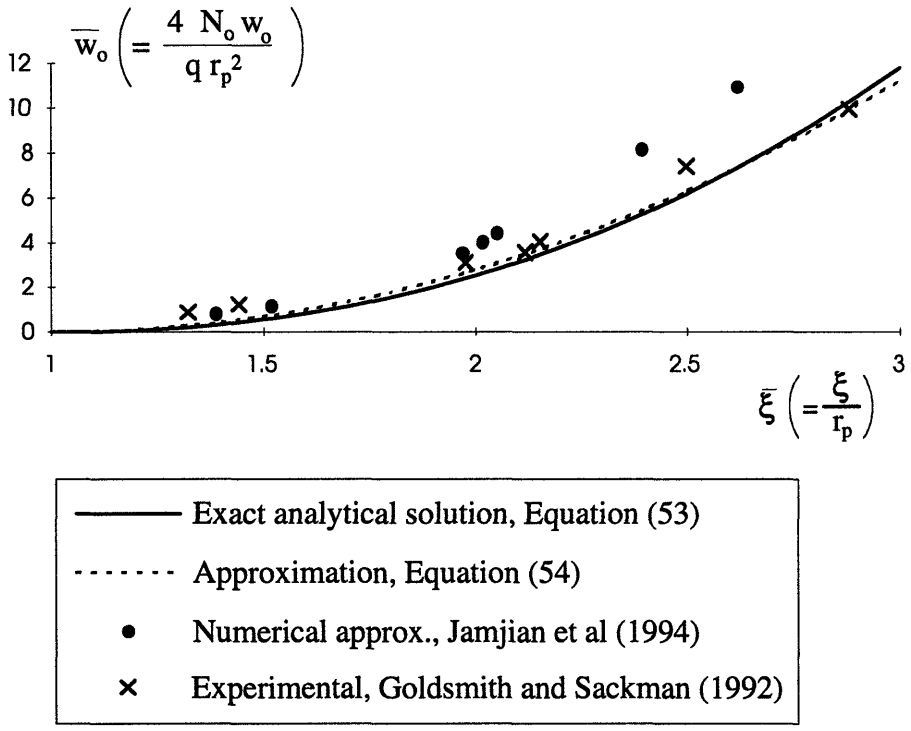

Figure 6: Comparison of present analytical solution for the central deflection of the facesheet to the numerical predictions of Jamjian et al. (1994) and the experimental results of Goldsmith and Sackman (1992).

4. ELASTIC, ISOTROPIC FACESHEET OVER A RIGID-PLASTIC FOUNDATION

This problem will be solved using equilibrium equations and energy methods in polar and rectangular coordinates, respectively. The reason for solving the problem in both ways will become apparent when a closed-form solution for the elastic, isotropic facesheet is presented.

4.1. FORMULATION IN POLAR COORDINATES

The sandwich structure is composed by two elastic, homogeneous, and isotropic facesheets and a fully-plastic honeycomb core. The plate is considered to be infinite, with facesheet thickness h, and honeycomb thickness H as shown in Figure 7. The facesheet is characterized by the Young's modulus E, and Poisson's ratio ν . During impact, the shear transmitted by the core to the facesheet is denoted q_r, and the crushing resistance of the honeycomb is denoted q_z. The problem to be solved is that of the local effect of a quasi-static punch load acting at the center of a circular sandwich plate when the deflections are large compared to the thickness of the facesheets. The same moving boundary conditions as in the fully-plastic, isotropic facesheet are applied at the extent of deformation.

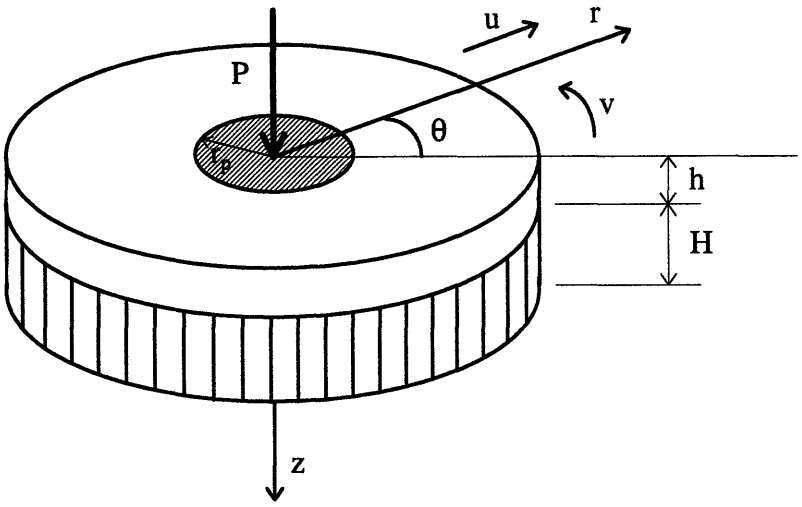

Figure 7: Geometry of the sandwich plate under a punch load in polar coordinates.

4.1.1. Solution

Recall from Chapter 3 that the governing differential equation for the vertical deflection of the facesheet to be solved is

$$\frac{\partial}{\partial r}\left(rN_r \frac{\partial w}{\partial r}\right) = q_z r. \tag{66}$$

Integrating Equation (66) with respect to the radial coordinate r gives

$$N_r \frac{\partial w}{\partial r} = \frac{q_z r}{2} + \frac{C_1}{r}, \tag{67}$$

where the integration constant C_1 is calculated using the first boundary condition

$$C_1 = -\frac{P}{2\pi}. \tag{68}$$

Rewriting Equation (67) after the introduction of the value of the integration constant C_1 gives

$$N_r \frac{\partial w}{\partial r} = \frac{q_z r}{2} - \frac{P}{2\pi r}. \tag{69}$$

where the extent of deformation ξ is function of the total indentation force P.

The relation between ξ and P can be calculated using the condition of kinematic continuity of the vertical deflection at the moving boundary. In a quasi-static problem, the monotonically increasing load can be considered a time-like parameter and used to substitute the time in the Equation (66)

$$\frac{\partial w}{\partial P} + \frac{\partial \xi}{\partial P}\frac{\partial w}{\partial r} = 0 \quad \text{at } r = \xi. \tag{70}$$

The relation between the total indentation load and the extent of deformation is obtained combining this kinematic continuity condition, Equation (70), with the first boundary condition of the problem

$$P = \pi q_z \xi^2. \tag{71}$$

Introducing the expression of the membrane force in the radial direction as a function of the vertical deflection, Equation (26), into Equation (69) gives

$$C\left(\frac{\partial w}{\partial r}\right)^3 = q_z r - \frac{P}{\pi r}. \tag{72}$$

where $C = \frac{Eh}{1-\nu^2}$ is the extensional rigidity. Finally, rewriting Equation (72) to get an expression of the slope results in

$$\frac{\partial w}{\partial r} = \sqrt[3]{\frac{1}{C}\left(q_z r - \frac{P}{\pi r}\right)}. \tag{73}$$

If Equation (73) is integrated with respect to r, the central deflection of the facesheet is obtained in terms of the total indentation load and the extent of deformation

$$w = \int_{r_p}^{r} \sqrt[3]{\frac{1}{C}\left(q_z r - \frac{P}{\pi r}\right)} dr - \int_{r_p}^{\xi} \sqrt[3]{\frac{1}{C}\left(q_z r - \frac{P}{\pi r}\right)} dr. \tag{74}$$

Since this equation can not be integrated directly, it will be solved by numerical integration using a computer code based in the trapezoidal method. The central deflection w_o can be calculated in the special case of a point load by setting $r_p = 0$ in Equation (74)

$$w_o = -\int_{0}^{\xi} \sqrt[3]{\frac{1}{C}\left(q_z r - \frac{P}{\pi r}\right)} dr. \tag{75}$$

4.1.2. Results

The objective of this analysis is to validate the approximate energy method that will be used for orthotropic plates. The comparison is done for elastic plates since analytical solutions can be derived using both approaches.

To compare the predictions using both equilibrium equations in a polar coordinate system and an approximate energy method in a rectangular coordinate system, the results will be particularized for four different cases. Two different facesheet laminates and two different honeycomb materials are combined to get different variations of the parameters involved. The two laminates are a [0/90] graphite/epoxy (Hercules AW193-PW prepreg consisting of AS4 fibers in a 3501-6 matrix) and a [0/90] kevlar/epoxy. Although these facesheets are orthotropic instead of isotropic, an equivalent stiffness will be calculated. This equivalent Young's modulus is equal to the longitudinal stiffness and, since for both laminates the number of plies in the longitudinal direction is equal to that in the transverse direction, is also equal to the transverse stiffness ($E_q = E_L = E_T$). The two cores selected are aramid paper honeycomb (HRH 10 1/8 - 3.0 Nomex with 1 in thickness from Ciba-Geigy) and aluminum honeycomb (1/8 - 5052 - 0.002 with 0.75 in thickness from Hexcel Corporation). The equivalent stiffnesses are calculated using an especially designed Microsoft Excel spreadsheet (printout included in appendix A). The crushing resistance of the aluminum honeycomb has been taken from data used by Goldsmith and Sackman [15] in their experimental work. Finally, the crushing resistance of the aramid paper honeycomb is estimated from a experimental plot of the load versus indentation (Williamson [23]) knowing the sizes of the test samples used (102 x 102 mm). Table 3 includes the parameters corresponding to each of the combinations.

	Facesheet		Honeycomb core	
Case	Material	E_0 (N/mm^2)	Material	q_z (N/mm^2)
1	Graphite/epoxy	77220	Nomex	1.389
2	Graphite/epoxy	77220	Aluminum	5.723
3	Kevlar/epoxy	40527	Nomex	1.389
4	Kevlar/epoxy	40527	Aluminum	5.723

Table 3: Facesheet and core combinations used to compare the results obtained using equilibrium equations and energy method.

The vertical deflection values obtained by using Equation (75) for each of the cases mentioned are shown in Figure 8.

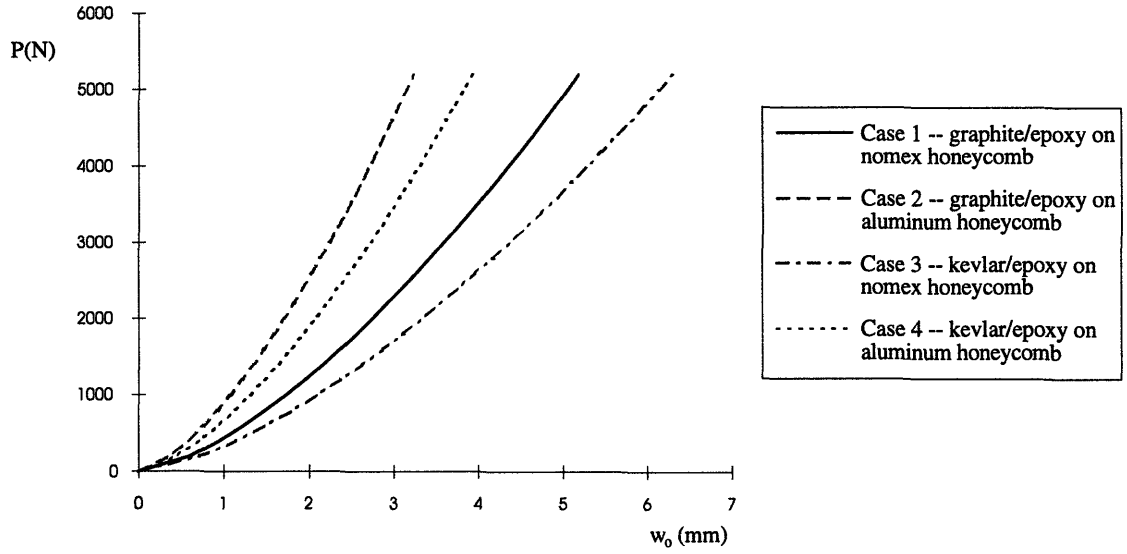

Figure 8: Vertical deflection versus total indentation force response for the four combinations of facesheets laminates and honeycomb cores proposed for the comparison of the equilibrium equations and energy method solutions.

4.2. FORMULATION IN RECTANGULAR COORDINATES

The sandwich structure is composed by two elastic, homogeneous, and isotropic facesheets and a rigid-plastic honeycomb core. The plate is considered to be infinite, with facesheet thickness h, and honeycomb thickness H as shown in Figure 9. The facesheet is characterized by the Young's modulus E, and Poisson's ratio ν. The crushing resistance of the honeycomb is denoted q_z. The problem to be solved is that of the local effect of a quasi-static punch load acting at the center of a rectangular sandwich plate when the deflections are large compared to the thickness of the facesheets.

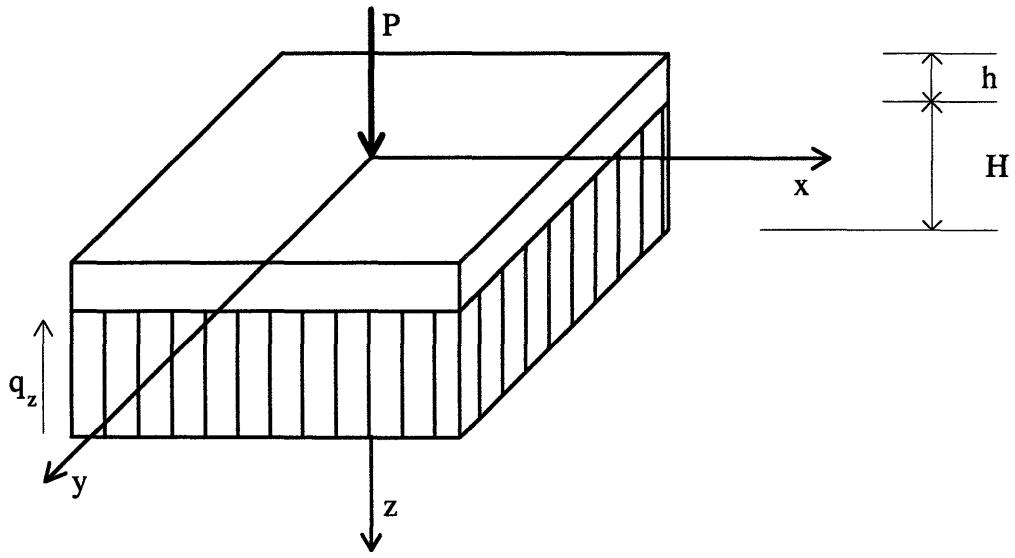

Figure 9: Geometry of the sandwich plate under the punch load where P is the total indentation force.

4.2.1. Approximate solution by energy method

Since the equilibrium equations for this problem derived in a non-linear differential equation that can not be solved directly, the Raleigh - Ritz method will be used to calculate an approximate solution. This method is based in the theory of stationary potential energy

$$\delta\Pi = 0, \tag{76}$$

where

$$\Pi = U - W. \tag{77}$$

U is the internal strain energy due to bending moments and membrane forces and W is the work done by applied external forces. For large deflections, the internal energy will include only the membrane term because bending moments are negligible when compared to membrane forces

$$U = U_m + U_b \cong U_m, \tag{78}$$

where

$$U_m = \frac{1}{2}\iint \left(N_x\varepsilon_x + N_y\varepsilon_y + N_{xy}\gamma_{xy}\right)dxdy. \tag{79}$$

Introducing the expressions of the membrane forces in terms of the normal and shear strains, Equations (6), into Equation (79) gives

$$U = \frac{1}{2} C \iint \left(\varepsilon_x^{\,2} + \varepsilon_y^{\,2} + 2\nu\varepsilon_x\varepsilon_y + \frac{1}{2}(1-\nu)\gamma_{xy}^{\,2} \right) dxdy, \tag{80}$$

where $C = \dfrac{Eh}{1-\nu^2}$ is the extensional rigidity. Applying the third assumption that states that the deformation of the faceplate takes place only in the vertical direction (u , v ≈ 0) and introducing the strain-displacement relationships, Equations (3), gives

$$U = \frac{1}{2} C \iint \frac{1}{4} \left[\left(\frac{\partial w}{\partial x} \right)^2 + \left(\frac{\partial w}{\partial y} \right)^2 \right]^2 dxdy. \tag{81}$$

On the other hand, W includes the work done by the total indentation load P, and the crushing resistance of the honeycomb

$$W = Pw_o - \iint q_z w dxdy, \tag{82}$$

where w_o is the deflection at the midpoint of the plate (x = 0 , y = 0).

4.2.1.1. Solution

To minimize the error resulting from the use of an approximate energy method, it is important to choose an appropriate shape function. The exact solution derived in polar coordinates from equilibrium equations can be used to plot the profile of the deformed

facesheet when subjected to the punch load. This profile suggests the use of a parabolic shape function

$$w = w_o\left[1 - \frac{x}{\xi}\right]^2\left[1 - \frac{y}{\xi}\right]^2. \tag{83}$$

The comparison between this selected shape function and the one calculated from Equation (74) using equilibrium equations and polar coordinates can be seen in Figure 10 for one particular value of the load. Similar results are obtained for different loads.

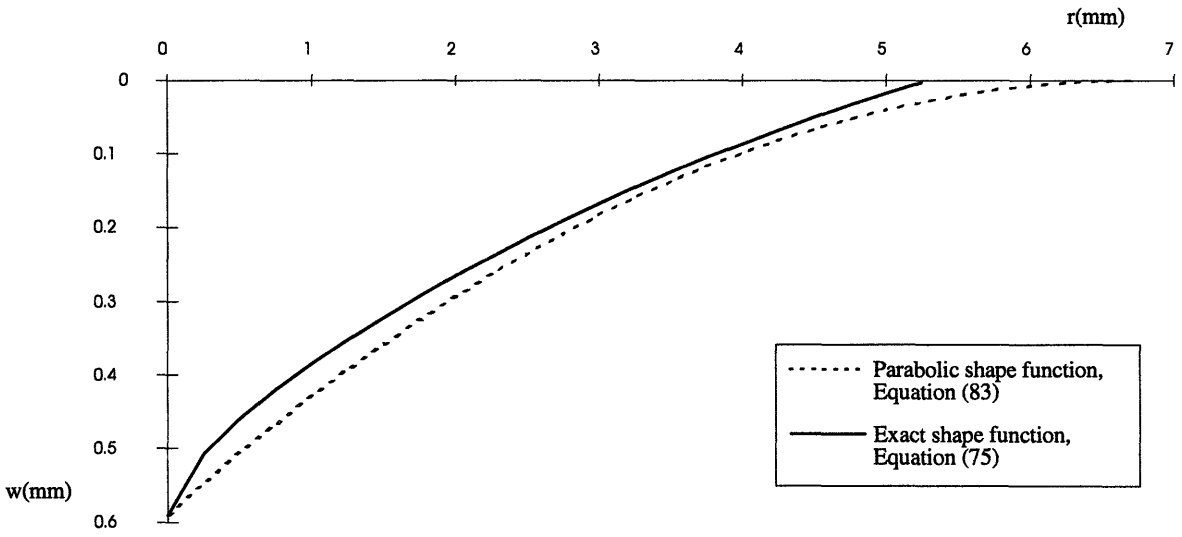

Figure 10: Comparison between the exact shape function obtained from the equilibrium equations in polar coordinates and the selected parabolic function.

Introducing the shape function given by Equation (83) into the expressions for the internal strain energy given by Equation (81) and work done by external forces given by Equation (82) results in

$$U = \frac{1}{2} C \int_0^{\xi} \int_0^{\xi} \left(\frac{w_o 2}{\xi} \right)^4 \left[\left[\left(1 - \frac{x}{\xi} \right) \left(1 - \frac{y}{\xi} \right)^2 \right]^2 + \left[\left(1 - \frac{y}{\xi} \right) \left(1 - \frac{x}{\xi} \right)^2 \right]^2 \right]^2 dxdy \quad (84)$$

and

$$W = Pw_o - \int_0^{\xi} \int_0^{\xi} q_z w_o \left[\left(1 - \frac{x}{\xi} \right)^2 \left(1 - \frac{y}{\xi} \right)^2 \right] dxdy . \quad (85)$$

The results after integration are

$$U = \frac{188}{2205} \frac{8Cw_o^4}{\xi^2} \quad (86)$$

and

$$W = Pw_o - \frac{4}{9} q_z w_o \xi^2 . \quad (87)$$

The total potential energy is calculated by adding the two terms integrated above

$$\Pi = \frac{188}{2205} \frac{8Cw_o^4}{\xi^2} - Pw_o + \frac{4}{9} q_z w_o \xi^2 . \quad (88)$$

Since Equation (88) must stationary for equilibrium

$$\frac{\partial \Pi}{\partial w_o} = \frac{188}{2205}\frac{32Cw_o^3}{\xi^2} + \frac{4}{9}q_z\xi^2 - P = 0. \tag{89}$$

From this previous condition, the total indentation load P is obtained in terms of the extent of deformation and the central vertical deflection

$$P = \frac{188}{2205}\frac{32Cw_o^3}{\xi^2} + \frac{4}{9}q_z\xi^2. \tag{90}$$

This expression, Equation (90), can be minimized with respect to ξ to obtain a new relationship between the vertical deflection and the extent of deformation

$$\frac{\partial P}{\partial \xi} = \frac{188}{2205}\frac{32Cw_o^3}{\xi^2} - \frac{4}{9}q_z\xi^2 = 0. \tag{91}$$

Finally, introducing Equation (91) into Equation (90) gives

$$P = \frac{8}{9}q_z\xi^2. \tag{92}$$

This relation allows the calculation of the extent of deformation as a function of the total indenting force. The result is introduced in Equation (90) to calculate the central deflection of the facesheet

$$w_o = \sqrt[3]{\frac{19845}{96256}\frac{P^2}{Cq_z}} = 0.59\sqrt[3]{\frac{P^2}{Cq_z}}. \tag{93}$$

4.2.2. Results

Using this one term approximation, the results from both equilibrium equations in polar coordinates and energy method in rectangular coordinates are compared in Figures 11 to 14. Each figure corresponds to one of the cases proposed in section 4.1.2.

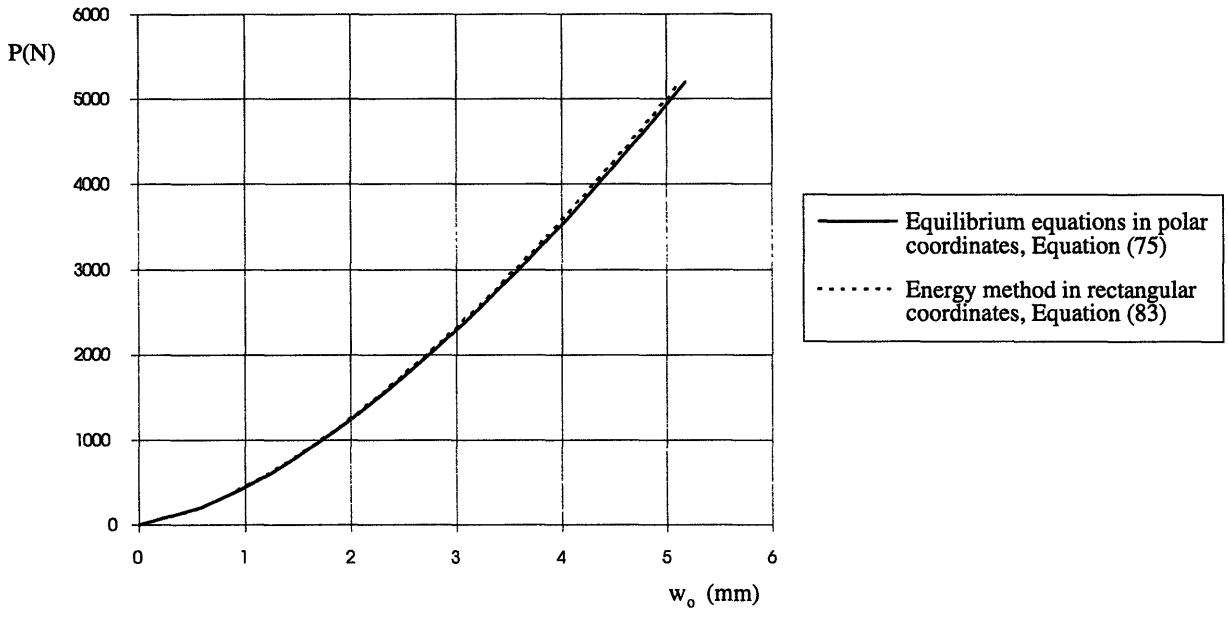

Figure 11: Comparison between the results from equilibrium equations in polar coordinates and those from the approximate energy method in rectangular coordinates. Case 1: graphite/epoxy on nomex honeycomb.

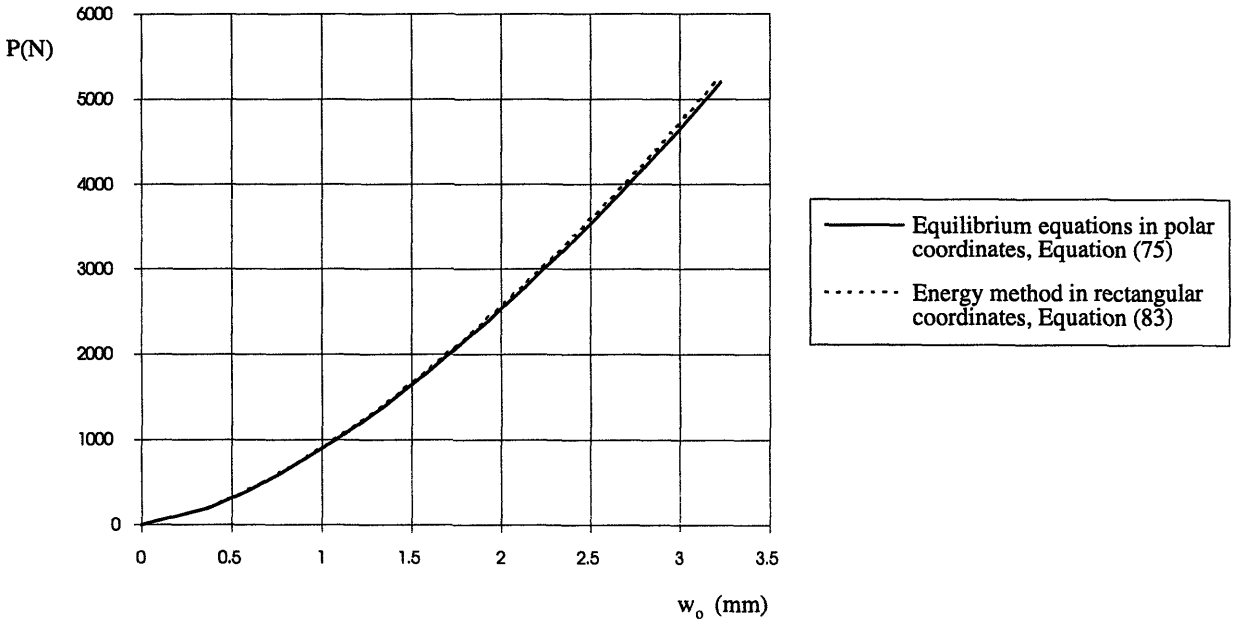

Figure 12: Comparison between the results from equilibrium equations in polar coordinates and those from the approximate energy method in rectangular coordinates. Case 2: graphite/epoxy on aluminum honeycomb.

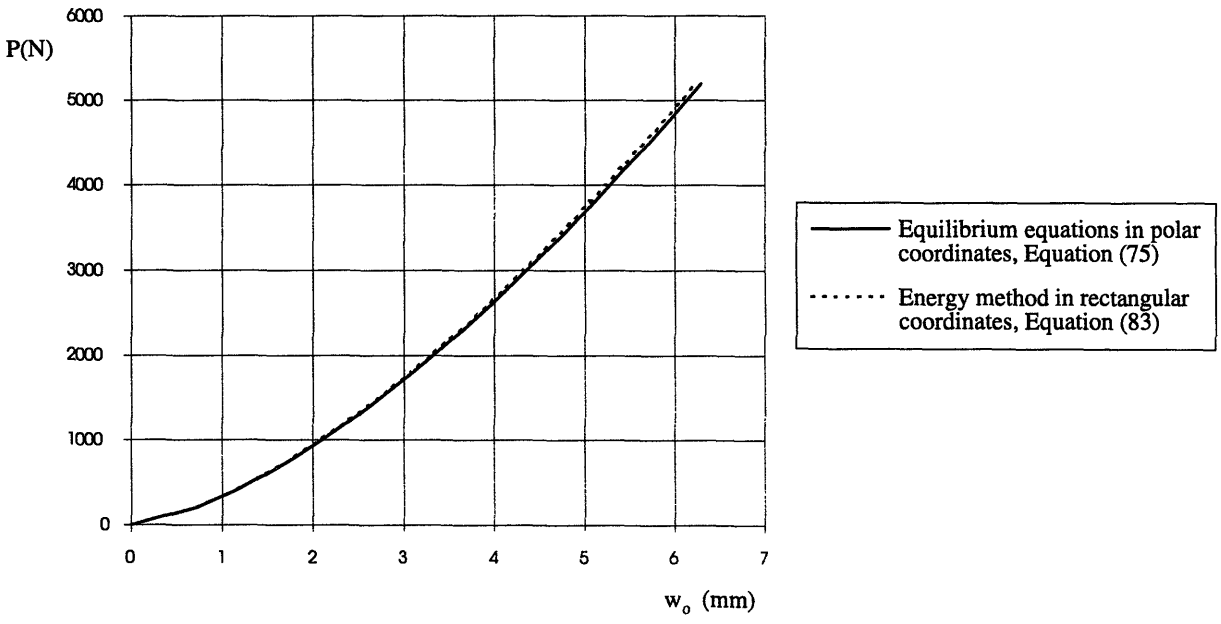

Figure 13: Comparison between the results from equilibrium equations in polar coordinates and those from the approximate energy method in rectangular coordinates. Case 3: kevlar/epoxy on nomex honeycomb.

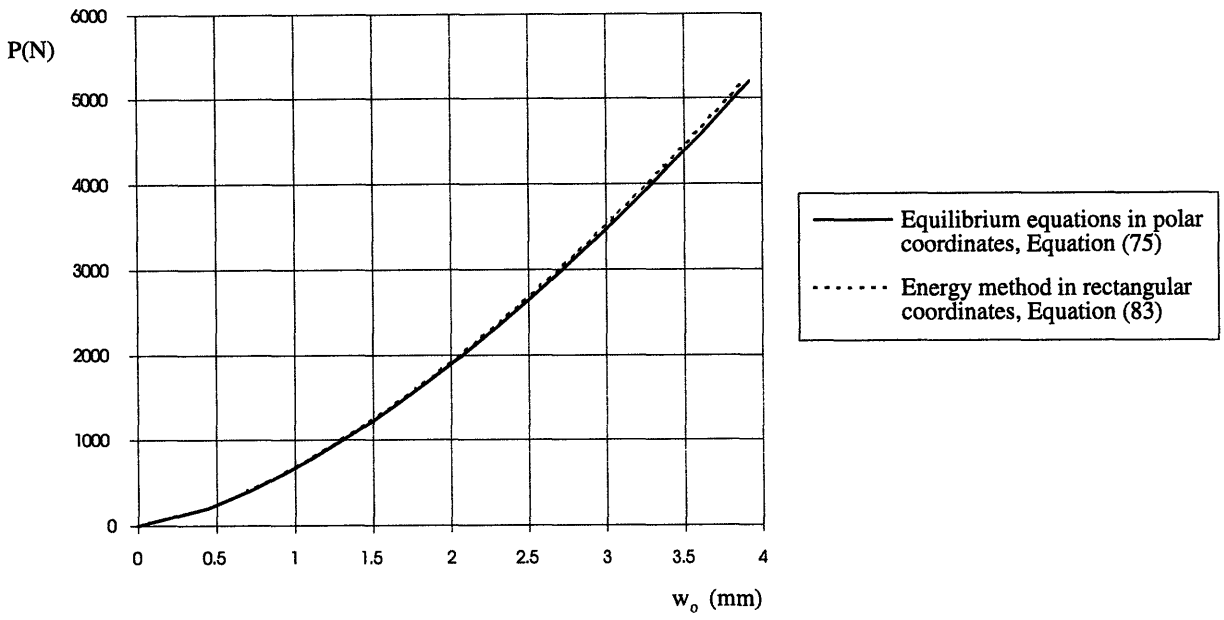

Figure 14: Comparison between the results from equilibrium equations in polar coordinates and those from the approximate energy method in rectangular coordinates. Case 4: kevlar/epoxy on aluminum honeycomb.

The results shown in Figures 11 to 14 confirm that the chosen shape function gives an excellent agreement with the exact solution derived in polar coordinates with only one term approximation. The error is less than 1% for all the cases considered. The same parabolic shape function will be used for the orthotropic facesheet.

5. ELASTIC, ORTHOTROPIC FACESHEET OVER A RIGID-PLASTIC FOUNDATION

The sandwich structure is composed of two elastic, homogeneous, and orthotropic facesheets and a rigid-plastic honeycomb core. The plate is considered to be infinite, and of facesheet thickness h, and honeycomb thickness H, as shown Figure 15. The facesheet is characterized by the longitudinal E_L and transversal E_T stiffnesses, and Poisson's ratio ν_{LT}. The crushing resistance of the honeycomb is denoted q_z. The problem to be solved is that of the local effect of a quasi-static punch load acting at the center of a rectangular sandwich plate when the deflections are large compared to the thickness of the facesheets.

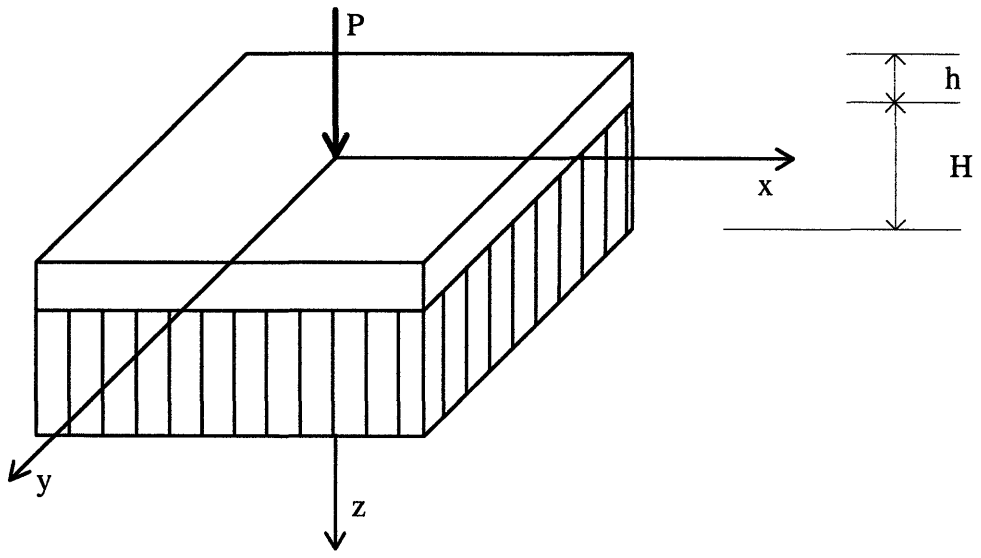

Figure 15: Geometry of the sandwich plate under the punch load where P is the total indenting force.

Since the assumptions made in solving the impact response of the rectangular isotropic plate are the same that those needed for an orthotropic facesheet, they will not be

repeated in the derivation of the solution. The equilibrium and strain-displacement equations are also the same for the isotropic and the orthotropic facesheets. However, the relationships between the membrane forces per unit length and the strains are rederived using the laminate theory.

5.1. EQUILIBRIUM OF FORCES AND MOMENTS

Laminate plate theory will be used to derive the relationship between membrane forces and strains for the special case of an orthotropic laminate.

The derivation begins by establishing relationships at the ply level that will be later extended to the laminate level. Two different coordinate systems are defined on the ply: a ply coordinate system with the longitudinal axis in the same direction as the fibers, and a laminate coordinate system established for the complete laminate as shown in Figure 16. Therefore, two different relations between stresses and strains are derived for each ply.

The relation between stresses and strains in the ply coordinate system (indexed by numbers) is

$$\begin{bmatrix} \sigma_1 \\ \sigma_2 \\ \sigma_6 \end{bmatrix} = \begin{bmatrix} Q_{11} & Q_{12} & 0 \\ Q_{21} & Q_{22} & 0 \\ 0 & 0 & Q_{66} \end{bmatrix} \begin{bmatrix} \varepsilon_1 \\ \varepsilon_2 \\ \varepsilon_6 \end{bmatrix}, \tag{94}$$

where the elements of the Q matrix are calculated from the properties of a single ply

$$Q_{11} = \frac{E_L}{1 - \nu_{LT}^{\,2} \dfrac{E_T}{E_L}} \tag{95}$$

$$Q_{22} = \frac{E_T}{1 - \nu_{LT}^{\,2} \frac{E_T}{E_L}} \tag{96}$$

$$Q_{12} = Q_{21} = \frac{\nu_{LT} E_T}{1 - \nu_{LT}^{\,2} \frac{E_T}{E_L}} \tag{97}$$

$$Q_{66} = G_{LT}. \tag{98}$$

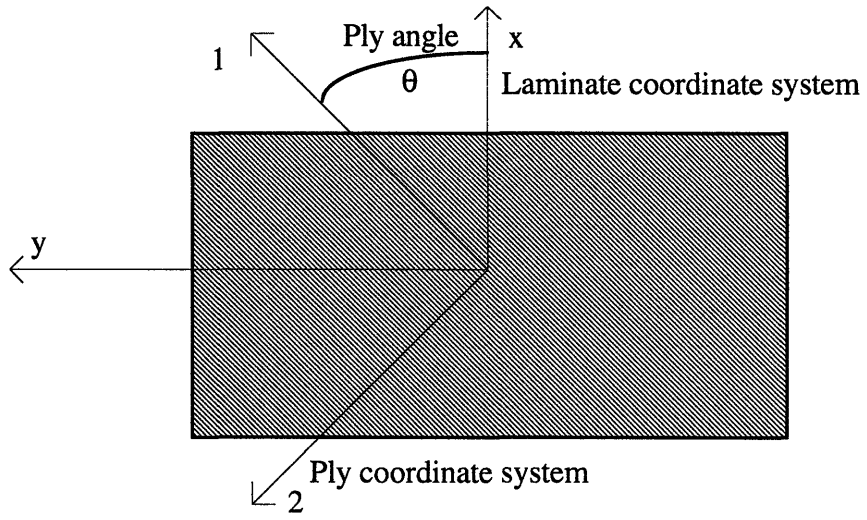

Figure 16: Coordinate systems on the laminate.

On the other hand, the same relation for the laminate coordinate system (denoted by an overline) is

$$\begin{bmatrix} \overline{\sigma_x} \\ \overline{\sigma_y} \\ \overline{\tau_{xy}} \end{bmatrix} = \begin{bmatrix} \overline{Q_{11}} & \overline{Q_{12}} & 0 \\ \overline{Q_{21}} & \overline{Q_{22}} & 0 \\ 0 & 0 & \overline{Q_{66}} \end{bmatrix} \begin{bmatrix} \overline{\varepsilon_x} \\ \overline{\varepsilon_y} \\ \overline{\gamma_{xy}} \end{bmatrix}. \tag{99}$$

The elements 16, 26, 61 and 62 of the Q matrices in both coordinate systems are zero due to the orthotropy of the facesheet.

A transformation of coordinates from the ply to the laminate relates these two Q matrices (ply and laminate)

$$\left[\overline{Q}\right] = \left[T_\theta^{-1}\right]\left[Q\right]\left[T_\theta^{-1}\right]^T, \tag{100}$$

where the transformation matrix T for a given ply angle θ is given by

$$T_\theta^{-1} = \begin{bmatrix} \cos^2\theta & \sin^2\theta & -2\sin\theta\cos\theta \\ \sin^2\theta & \cos^2\theta & 2\sin\theta\cos\theta \\ \sin\theta\cos\theta & -\sin\theta\cos\theta & \cos^2\theta - \sin^2\theta \end{bmatrix}. \tag{101}$$

The in-plane forces per unit length of the ply are equal to the stresses on the laminate coordinate system times the thickness of the ply t

$$N_x = \sigma_x t \tag{102}$$

$$N_y = \sigma_y t \tag{103}$$

$$N_{xy} = \tau_{xy} t. \tag{104}$$

When all the plies are bonded together to form a laminate, the in-plane forces per unit length are equal to the sum of the forces on each of the plies

$$N_x = \sum_{k=1}^{N} \sigma_x^k t_k \tag{105}$$

$$N_y = \sum_{k=1}^{N} \sigma_y^k t_k \tag{106}$$

$$N_{xy} = \sum_{k=1}^{N} \tau_{xy}^k t_k , \tag{107}$$

where the stresses of each of the plies are defined according to Equation (99)

$$\overline{\sigma^{(k)}} = \left[\overline{Q_k}\right]\overline{\varepsilon_k} . \tag{108}$$

In an ideal laminate all the plies are perfectly bonded. Therefore, the strains of all plies must be equal and equal to the strains of the laminate. This assumption allows the simplification:

$$N = \sum_{k=1}^{N} \left[\overline{Q_k}\right]\overline{\varepsilon_k} t_k = \left[\sum_{k=1}^{N} \left[\overline{Q_k}\right] t_k\right] \varepsilon . \tag{109}$$

Finally, Equation (109) is written in matrix form

$$\begin{bmatrix} N_x \\ N_y \\ N_{xy} \end{bmatrix} = [A] \begin{bmatrix} \varepsilon_{xo} \\ \varepsilon_{y_o} \\ \gamma_{xy_o} \end{bmatrix}, \tag{110}$$

where

$$A = \sum_{k=1}^{N} \left[\overline{Q_k}\right] t_k . \tag{111}$$

5.2. APPROXIMATE SOLUTION BY ENERGY METHOD

The equilibrium equations for this problem result in a non-linear differential equation that can not be solved directly. A Raleigh - Ritz energy method will be used to calculate an approximate solution. The methodology needed for the orthotropic facesheet is the similar to the one derived for the isotropic solution.

The internal energy due to membrane forces was defined as

$$U = \frac{1}{2} \iint \left(N_x \varepsilon_x + N_y \varepsilon_y + N_{xy} \gamma_{xy} \right) dxdy . \tag{112}$$

When the relation between membrane forces and strains for composite materials given by Equation (110) is introduced into the expression of the internal energy due to membrane forces given by Equation (112), a new expression of the elastic strain energy that takes into account the directionality of the properties in the laminate is obtained

$$U = \frac{1}{2} \iint \left(A_{11} \varepsilon_x^2 + 2 A_{12} \varepsilon_x \varepsilon_y + A_{22} \varepsilon_y^2 + A_{66} \gamma_{xy}^2 \right) dxdy , \tag{113}$$

where A_{ij} are the elements of the A matrix defined in Equation (110).

A new relationship can be derived by applying the assumption which states that the deformation of the faceplate takes place only in the vertical direction (u , v ≈ 0) and introducing the strain-displacement relationships given by Equation (3)

$$U = \frac{1}{2}\iint\left[A_{11}\left(\frac{\partial w}{\partial x}\right)^4 + A_{22}\left(\frac{\partial w}{\partial y}\right)^4 + (2A_{12} + 4A_{66})\left(\frac{\partial w}{\partial y}\right)^2\left(\frac{\partial w}{\partial y}\right)^2\right]dxdy. \quad (114)$$

On the other hand, the total work W includes the work done by the total indentation load P and the crushing resistance of the honeycomb

$$W = Pw_o - \iint q_z w dxdy, \quad (115)$$

where w_o is the deflection at the midpoint of the plate (x = 0 , y = 0).

5.2.1. Solution

The same shape function selected for the isotropic facesheet in rectangular coordinates will be used again because of the excellent agreement with the exact solution given by equilibrium equations in polar coordinates. The faceplate deflection is assumed to be of the form

$$w = w_o\left[1 - \frac{x}{\xi}\right]^2\left[1 - \frac{y}{\xi}\right]^2. \quad (116)$$

The expressions for the internal strain energy given by Equation (114) and work done by external forces given by Equation (115) can be integrated with respect to x and y after the introduction of the shape function, Equation (116), to get

$$U = \frac{8w_o^4}{\xi^2}\left[\frac{1}{45}(A_{11} + A_{22}) + \frac{1}{49}(2A_{12} + 4A_{66})\right] \tag{117}$$

and

$$W = Pw_o - \frac{4}{9}q_z w_o \xi^2.$$

The integration limits are from $x = y = r_p = 0$ and the extent of deformation $x = y = \xi$. The lower limit is zero because a concentrated load is assumed. This assumption is valid if the contact area between the facesheet and the nose of the projectile is very small (as initially the case of a hemispherical-nosed projectile).

The total potential energy is calculated by adding the two terms integrated above

$$\Pi = \frac{8w_o^4}{\xi^2}\left[\frac{1}{45}(A_{11} + A_{22}) + \frac{1}{49}(2A_{12} + 4A_{66})\right] - Pw_o + \frac{4}{9}q_z w_o \xi^2. \tag{118}$$

Since the total energy be must be stationary for equilibrium $(\delta\Pi = 0)$,

$$\frac{\partial \Pi}{\partial w_o} = \frac{32w_o^3}{\xi^2}\left[\frac{1}{45}(A_{11} + A_{22}) + \frac{1}{49}(2A_{12} + 4A_{66})\right] - P + \frac{4}{9}q_z \xi^2 = 0. \tag{119}$$

From the above condition, the total indenting force P is obtained in terms of the extent of deformation and the central vertical deflection

$$P = \frac{32 w_o^3}{\xi^2}\left[\frac{1}{45}\left(A_{11} + A_{22}\right) + \frac{1}{49}\left(2A_{12} + 4A_{66}\right)\right] + \frac{4}{9} q_z \xi^2. \tag{120}$$

This Equation (120) can be minimized with respect to ξ to obtain a relationship between the vertical deflection and the extent of deformation

$$\frac{\partial P}{\partial \xi} = \frac{32 w_o^3}{\xi^2}\left[\frac{1}{45}\left(A_{11} + A_{22}\right) + \frac{1}{49}\left(2A_{12} + 4A_{66}\right)\right] - \frac{4}{9} q_z \xi^2 = 0. \tag{121}$$

Finally, introducing Equation (121) into Equation (120) gives

$$P = \frac{8}{9} q_z \xi^2. \tag{122}$$

This relation allows the calculation of the extent of deformation as a function of the total indenting force. Finally, Equation (122) is introduced in Equation (120) to give the central deflection of the facesheet as a function of the total indentation load

$$w_o = \sqrt[3]{\frac{9P^2}{512 q_z\left[\frac{1}{45}\left(A_{11} + A_{22}\right) + \frac{1}{49}\left(2A_{12} + 4A_{66}\right)\right]}}. \tag{123}$$

5.2.1. Introduction of impact parameters

The equations of the quasi-static approximation are still valid if the inertia of the facesheet can be neglected compared to the inertia of the projectile, i.e., the process is quasi-dynamic. If F_{plate} is the inertia of the facesheet and F_{proj} is the inertia of the projectile,

$$\frac{F_{plate}}{F_{proj}} << 1. \tag{124}$$

The relation between them was established in section 3.6.1.

$$\frac{F_{plate}}{F_{proj}} \leq \frac{\pi r_p^2 m}{M_o}\left(\frac{\xi}{r_p}\right)^2 = \frac{M_p}{M_o}\left(\frac{\xi}{r_p}\right)^2 \tag{125}$$

or when the applied load is concentrated at the center of the plate ($r_p = 0$)

$$\frac{F_{plate}}{F_{proj}} \leq \frac{m\pi\xi^2}{M_o}. \tag{126}$$

For the experimental values that Williamson [23] used in their tests, the maximum extent of deformation calculated is 50 mm, and the mass of the lightest projectile is 1.53 kg. The maximum ratio between the inertia of the plate and the inertia of the projectile is 0.003. Therefore, the problem is indeed "quasi-dynamic." This fact was also pointed by Williamson in his experimental work. He observed that the total indenting force versus the central deflection responses were similar for static and impact tests at low impact velocities performed over the same configuration.

Considering that the kinetic energy transmitted by the projectile to the facesheet is converted into plastic deformation of the honeycomb and elastic energy stored in the plate, an energy balance can be established to relate the extent of deformation and the central deflection with impact parameters.

The kinetic energy that the projectile transmits to the plate is function of its mass and initial speed

$$E_k = \frac{1}{2} M_o V_o^2. \tag{127}$$

On the other hand, the energy absorbed by the plate includes the energy required to crush the honeycomb plus the energy required to elastically deform the facesheet. It is calculated from the total indentation force

$$E = \int_0^{w_o} P(w_o) dw_o. \tag{128}$$

The result of the above integral gives

$$E = \frac{32}{15} w_o^{5/2} \sqrt{2 q_z \left[\frac{1}{45} (A_{11} + A_{22}) + \frac{1}{49} (2 A_{12} + 4 A_{66}) \right]}. \tag{129}$$

Finally, a relationship between the central deflection and the experimental parameters is obtained by equating both the kinetic energy communicated to the facesheet by the projectile and the energy absorbed in crushing the honeycomb and deforming the faceplate

$$E = \frac{32}{15} w_o^{5/2} \sqrt{2q_z \left[\frac{1}{45}(A_{11} + A_{22}) + \frac{1}{49}(2A_{12} + 4A_{66}) \right]} = \frac{1}{2} M_o V_o^2 = E_k, \quad (130)$$

or

$$w_o^{5/2} = \frac{15 M_o V_o^2}{64 \sqrt{2q_z \left[\frac{1}{45}(A_{11} + A_{22}) + \frac{1}{49}(2A_{12} + 4A_{66}) \right]}}. \quad (131)$$

Equation (131) allows the calculation of the vertical deflection of the facesheet as a function of the impact parameters. Moreover, once the central deflection is known, the total indentation force P and the extent of deformation ξ can also be calculated form Equations (122) and (123).

5.3. DESCRIPTION OF THE EXPERIMENTAL WORK

The present analysis is correlated with the experimental results from J.E. Williamson [23]. Static indentation and impact tests were performed with hemispherical-nosed projectiles into both bare honeycomb and sandwich plates with graphite/epoxy facesheets and nomex honeycomb. In both sandwich configurations the targets were supported by a rigid foundation while the sandwich plate was also tested with two edges clamped.

The tests were subjected to the following conditions: the deformed area was much smaller than the lateral extent of the samples, the thickness of the core was limited to three

values, the diameter of the impactor was greater than cell dimensions and plate thickness, and impact velocities ranged from 1.20 to 3.45 m/s.

The material used was a Hercules AW193-PW prepreg consisting of AS4 graphite fibers in a plain weave impregnated with 3501-6 epoxy matrix as facesheets and Ciba-Geigy Nomex honeycomb with cell diameter of 3.2 mm and density of 48 kg/m^3 (HRH 10 1/8 - 3.0) as cores. The tests were performed with samples of different facesheet laminates ([0/90], [0/90/0], [0/90/0/90], and $[0/90]_{10}$) and core thicknesses (6.4, 9.5, and 25.4 mm), impactor diameters (12.7, 25.4, and 38.1 mm) , and support conditions (rigid foundation and two edges clamped).

5.4. RESULTS

The material properties of the AS4/3501-6 system needed for the calculation of the A matrix are

$$E_L = 142 \text{ KN/mm}^2$$

$$E_T = 9.8 \text{ KN/mm}^2$$

$$G_{LT} = 7.1 \text{ KN/mm}^2$$

$$\nu_{LT} = 0.3.$$

These properties were taken from Tsai [5] for unidirectional tapes.

Since Williamson and Tsang [24] used exactly the same material for their experimental work, these properties were checked against data given by Tsang for the [0/90] plain weave laminate. The first step was the calculation of the A matrix for the laminate with a Microsoft Excel spreadsheet especially designed for that task. The printouts are included in Appendix A. The result for the [0/90] laminate is

$$[A]_{[0/90]} = \begin{bmatrix} 26731 & 1035.43 & 0 \\ 1035.43 & 26731 & 0 \\ 0 & 0 & 2485 \end{bmatrix} \text{(N/mm)}.$$

The engineering longitudinal and transverse equivalent stiffnesses are calculated using

$$E_L = \frac{1}{ha_{11}} \tag{132}$$

$$E_T = \frac{1}{ha_{22}} \tag{133}$$

$$\nu_{LT} = -\frac{a_{12}}{a_{11}} \tag{134}$$

$$G_{LT} = \frac{1}{ha_{66}}, \tag{135}$$

where a_{ij} are the elements of the $[a] = [A]^{-1}$ matrix. Since these calculations are for a laminate composed by unidirectional plies instead of a plain weave laminate, a correction factor will be applied. This factor is calculated from a relation between the calculated engineering constants for a laminate composed by unidirectional plies and a plain weave laminate for a similar T300/F934 graphite/epoxy system given by Tsai [5]. The result of

this comparison to the experimental data given by Tsang for the [0/90] plain weave AS4/3501-6 graphite/epoxy laminate are shown in Table 4.

	Present estimation	Experimental data, Tsang	Error (%)
E_L (N/mm^2)	63524.4	63800	0.86
E_T (N/mm^2)	63524.4	63600	0.12
G_{LT} (N/mm^2)	6326.1	6270	0.89

Table 4: Comparison between the present estimation of the engineering constants and the experimental data given by Tsang for the [0/90] plain weave laminate.

The A matrices for the [0/90/0] and [0/90/0/90] laminates which Williamson also used in his experimental work are

$$[A]_{[0/90/0]} = \begin{bmatrix} 51736.3 & 1553.15 & 0 \\ 1553.15 & 28456.8 & 0 \\ 0 & 0 & 3727.5 \end{bmatrix} \text{(N/mm)}$$

$$[A]_{[0/90/0/90]} = \begin{bmatrix} 53462.1 & 2070.86 & 0 \\ 2070.86 & 53462.1 & 0 \\ 0 & 0 & 4970 \end{bmatrix} \text{(N/mm).}$$

The printouts of the calculations for the A matrices are included in Appendix B.

Once the coefficients A_{ij} for the laminates are known, they are introduced into Equation (120) to get the values of the central deflection as a function of the total indenting force. Two different sets of results can be obtained for each of the laminates

([0/90], [0/90/0], and [0/90/0/90]): (1), those obtained by calculating the laminate as composed of unidirectional plies; and, (2), those obtained using the data for the [0/90] woven laminate given by Tsang [24]. These results will be compared to the experimental data with a double objective: first, to explore the influence of the diameter of the hemispherical nose of the projectile and check the assumption of a concentrated load, and, second, to validate the analytical predictions of the central deflections as a function of the total indenting force.

5.4.1. Influence of the tup diameter

The load was assumed concentrated at the middle of the plate because the contact radius is very small and difficult to estimate without knowing the exact shape of the deformed facesheet. The proportions can be seen in Figure 17 at the point of facesheet fracture for the [0/90] laminate and 25.4 mm core when a 12.7 mm diameter tup was used.

The predictions for the [0/90] laminate will be compared with the experimental results using three different tup diameters (12.7 mm, 25.4 mm, and 38.1 mm) to check the assumption of a concentrated load. The comparison can be seen in Figures 18 and 19.

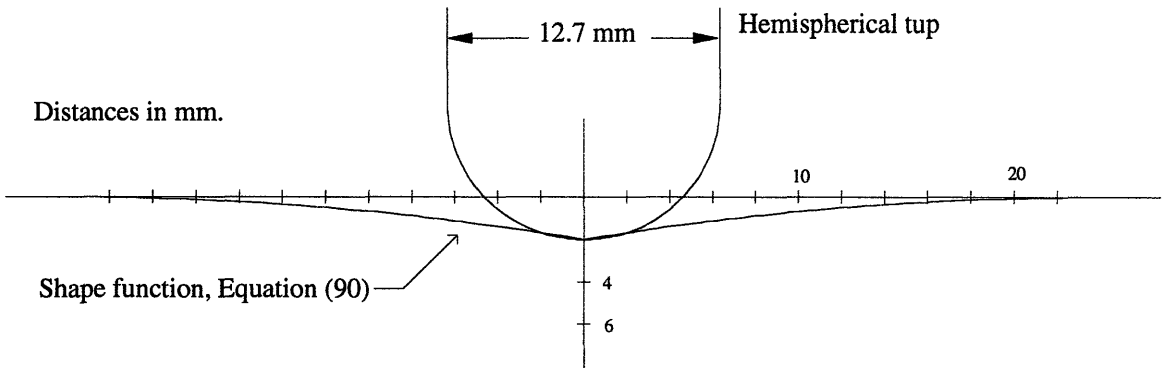

Figure 17: Shape function for the [0/90] laminate at the moment of fracture when the 12.7 mm tup is used.

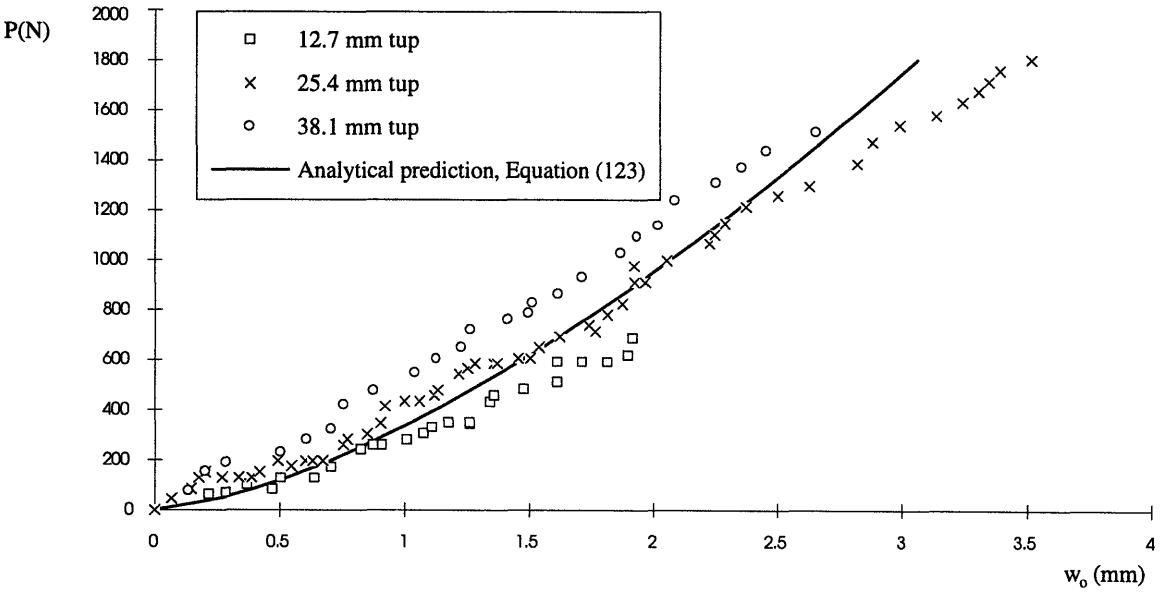

Figure 18: Total indentation load versus facesheet central deflection for a [0/90] facesheet and a 25.4 mm core. Comparison of the predicted values with the experimental results for 12.7 mm, 25.4 mm, and 38.1 mm hemispherical tups. The calculation is done by assuming that the laminate is composed of unidirectional plies.

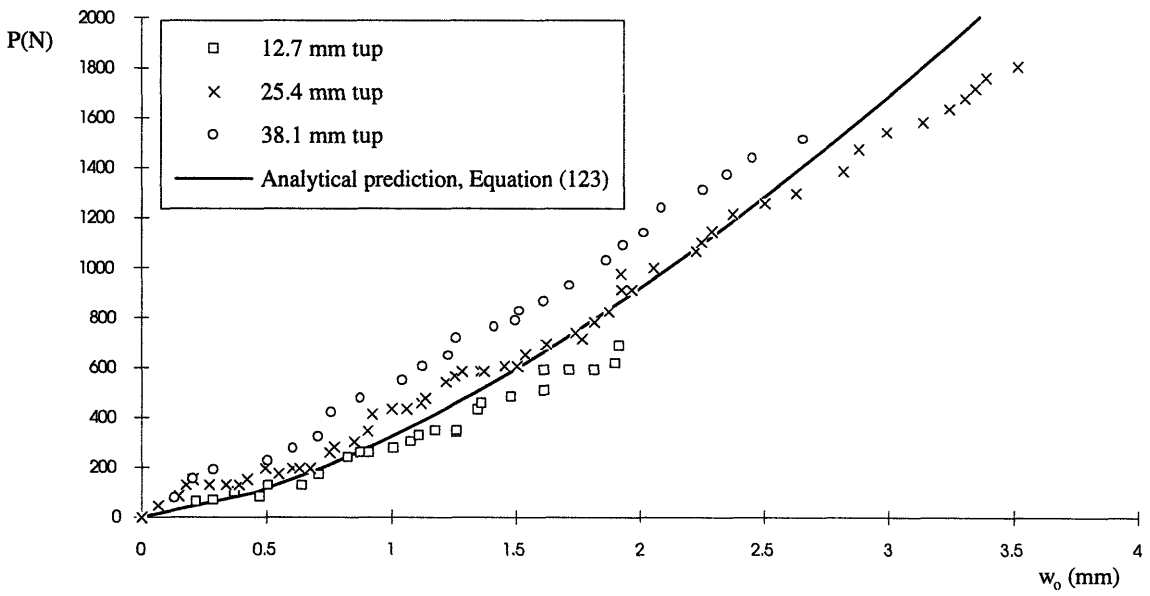

Figure 19: Total indentation load versus facesheet central deflection for a [0/90] facesheet and a 25.4 mm core. Comparison of the predicted values with the experimental results for 12.7 mm, 25.4 mm, and 38.1 mm hemispherical tups. The calculation is done using the data of the plain weave laminate given by Tsang (1994).

It can be seen in Figures 18 and 19 that the analytical predictions in both cases show an excellent agreement with the experimental data for small indentations or small contact areas. The results, as expected, are closer to the data of the tup with the smallest diameter where the load is more concentrated, the 12.7 mm tup.

5.4.2. Prediction of the central deflection as a function of the total indenting force

The plots of the central deflection versus the total indenting force for the [0/90/0] and [0/90/0/90] facesheets and 25.4 mm core when impacted by a 25.4 mm diameter tup are shown in Figures 20 and 21. The results for the [0/90] facesheet and 25.4 mm core are in Figures 18 and 19. The results obtained by using plain weave data from Tsang [24] have been also included for the [0/90/0/90] laminate.

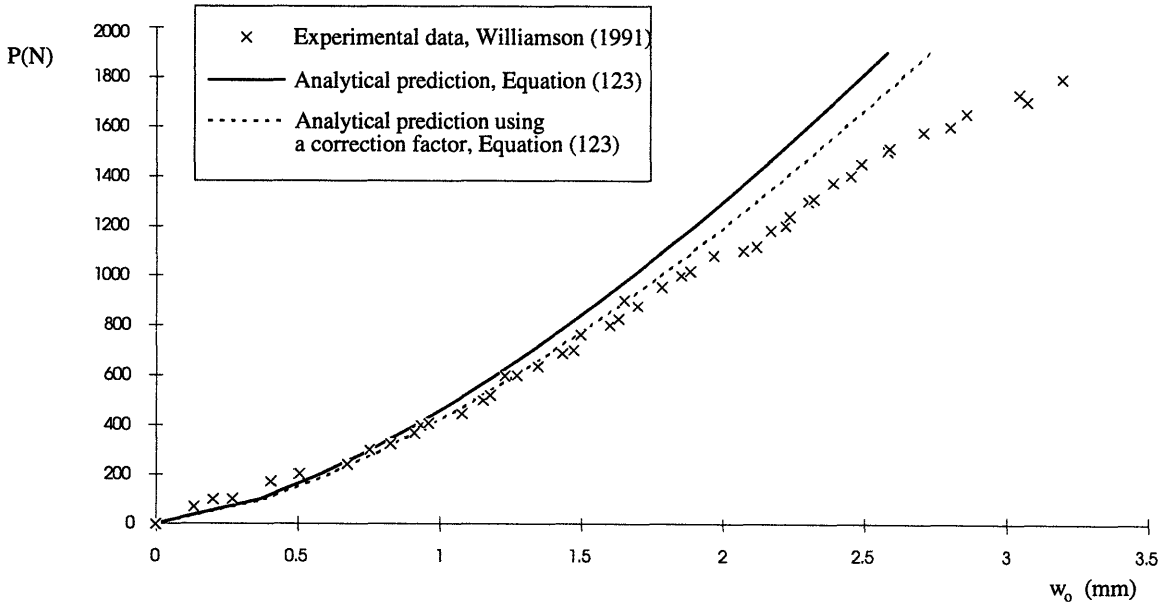

Figure 20: Total indentation load versus central deflection of the facesheet for a [0/90/0] facesheet and a 25.4 mm core. Comparison between the experimental results of Williamson (1991) and the analytical solutions. The diameter of the tup is 25.4 mm.

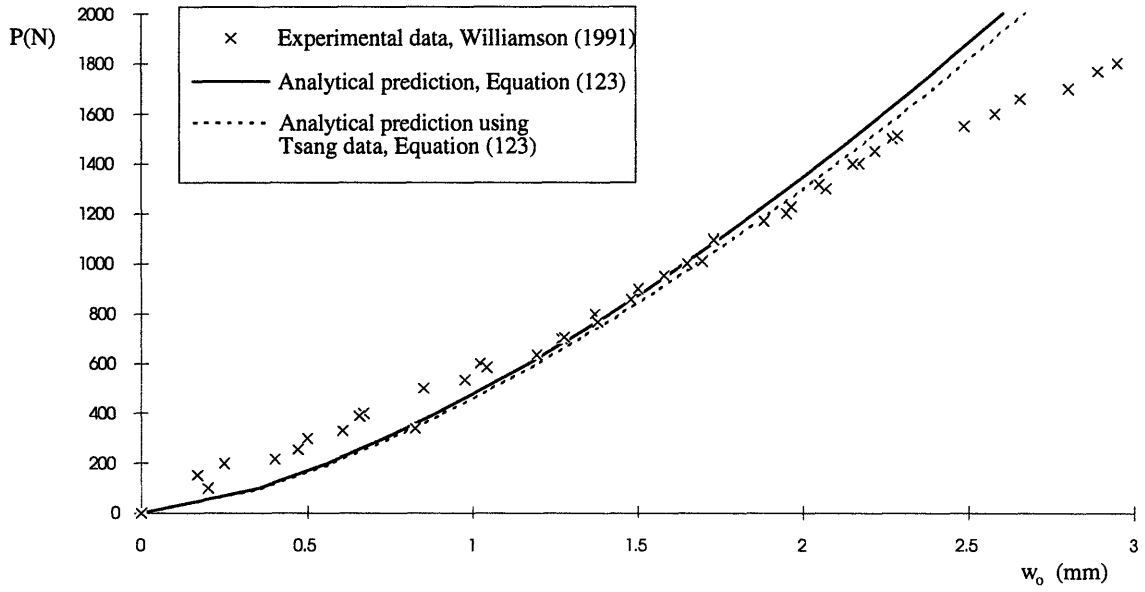

Figure 21: Total indentation load versus facesheet central deflection for a [0/90/0/90] facesheet and a 25.4 m core. Comparison between the experimental results of Williamson (1991) and the analytical solutions. The diameter of the tup is 25.4 mm.

Figures 20 to 21 show that even with only one term approximation, the correlation between analytical results and experimental data is very good. Except for small values of the indentation, the analytical predictions are within 10% of the experimental results. The high disparity between the analytical solutions and the experimental data observed for small values of the facesheet indentation shows that bending resistance is not negligible compared to membrane resistance when the deflections are of the order of the facesheet thickness. The percentage difference also increases slightly with the total indentation force due to the increase of the contact area between the deformed facesheet and the hemispherical nose of the projectile as the faceplate deforms.

6. CONCLUSION AND RECOMMENDATIONS

The primary objective of this thesis was to develop simple closed-form solutions for the local impact response of sandwich panels. These equations may be a valuable tool for designers since they relate the local indentation of the panel to the projectile mass and velocity, and the geometric and material properties of the sandwich. Analytical solutions were presented for three different sandwich configurations: a fully-plastic, isotropic facesheet, an elastic, isotropic facesheet, and an elastic, orthotropic facesheet, all with honeycomb cores. Where possible, these solutions were correlated to experimental data in order to test the validity of the assumptions made, to show the accuracy of the analytical model, and to limit the applicability of the theory. Each of the above mention configurations will be discussed separately below.

A simple closed-form solution for the plate indentation was obtained for the fully-plastic, isotropic faceplate when subjected to impact of flat-nosed projectiles traveling at low velocities. The equilibrium equations were solved for an indentation load used to represent the projectile impact. The load indentation response was then used to estimate the plastic work required to plastically deform the plate and to crush the honeycomb. A relationship was then obtained for the indentation as a function of the mass and velocity of the projectile by using an energy balance between the kinetic energy of the projectile and the plastic work. The central deflection of the facesheet and the extent of deformation were predicted for seven aluminum facesheet and aluminum honeycomb configurations with impact velocities in the range 10 to 40 m/s. The comparison between the experimental data and the analytical results for the central deflection gave errors within 5% except for the highest velocities where the value of error reached 16%. On the other hand, for the extent of deformation, the analytical results were within 8% error when compared to the experimental data except for tests with the highest impact velocities for which the error reached 19%.

An exact solution for the impact response of a sandwich composed of an elastic, isotropic facesheet was derived in polar coordinates from equilibrium equations. The solution for the plate deformation was then used to describe a shape function that was used in a Raleigh - Ritz energy method approximation of the same problem in rectangular coordinates. The exact solution suggested the use of a parabolic shape function. Using this shape function, it can be shown that the energy method approximation and the exact solution are within 1% of each other.

A simple closed-form solution for plate indentation was found for the sandwich composed of elastic, orthotropic facesheets and honeycomb core under low velocity impact of a hemispherical-nosed projectile. A solution using a one term Raleigh - Ritz energy approximation with the same parabolic shape function as in the above case was presented for the sandwich with elastic, orthotropic facesheets. As in the case of the fully-plastic facesheets, the plate indentation was related to the projectile mass and velocity and geometric and material properties of the sandwich. The predicted central deflection was within 10% of the experimental results on graphite/epoxy woven facesheets and nomex honeycombs performed under static indentation and impact loads. It was observed that the error decreased when the properties of the plain weave material were used instead of those of the unidirectional tapes of the same material. On the other hand, the error increased as the contact area between the projectile nose and the facesheet increased. Future research should address the influence of an increasing contact area as the plate deforms. Furthermore, knowledge of the load-deflection characteristics could be used to predict the initiation and propagation of cracks.

In both experiments with the fully-plastic, isotropic and elastic, orthotropic facesheets the mass of the deformed plate was in fact much lower than that of the projectile and the problem was indeed "quasi-dynamic." Furthermore, plate deflections in both cases were several times the thickness of the plate and negligible plate bending resistance was a reasonable assumption. The proposed solutions are therefore restricted to

impact scenarios in which the projectile has low velocity but high mass and causes indentations that are several times the thickness of the plate.

7. REFERENCES

1. Shenoi, R.A. and Wellicome, J.F., *Composite Materials in Maritime Structures, Volume 1 Fundamental Aspects*, Cambridge Ocean Technology Series, Cambridge University Press, Cambridge, Great Britain, 1993.

2. Shenoi, R.A. and Wellicome, J.F., *Composite Materials in Maritime Structures, Volume 2 Practical Considerations*, Cambridge Ocean Technology Series, Cambridge University Press, Cambridge, Great Britain, 1993.

3. Jones, R.M., *Mechanics of Composite Materials*, Hemisphere Publishing Corporation, 1975.

4. Lubin, G., *Handbook of Composites*, Van Nostrand Reinhold, New York, NY, 1982.

5. Tsai, S.W., *Theory of Composites Design*, Think Composites, Dayton, OH, 1992.

6. Raju, I.S. and Wang, J.T., "Classical Laminate Theory Models for Woven Fabric Composites", *Journal of Composites Technology & Research*, Vol. 16, No. 4, October 1994, pp. 289-303.

7. Allen, H.G., "The Story of Sandwich Construction", *1st Core Conference*, Zurich, Switzerland, 1988, pp.1-24.

8. Ericsson, A. and Sankar, B.V., "Contact Stiffness of Sandwich Plates and Application to Impact Problems", in *Sandwich Constructions 2 Volume I (Proceedings of the Second International Conference on Sandwich Constructions*, Gainesville, FL, March 9-12), ed. Weissman-Berman, D. and Olsson, K-A., Engineering Materials Advisory Services Ltd., West Midlands, Great Britain, 1992, pp. 139-159.

9. Hayman, B., Haug, T. and Valsgard, S., "Slamming Drop Tests on a GRP Sandwich Hull Model", in *Sandwich Constructions 2 Volume II (Proceedings of the Second International Conference on Sandwich Constructions*, Gainesville, FL, March 9-12), ed. Weissman-Berman, D. and Olsson, K-A., Engineering Materials Advisory Services Ltd., West Midlands, Great Britain, 1992, pp. 583-604.

10. Wierzbicki, T., Lacruz Alvarez, A. and Hoo Fatt, M.S., "Impact Energy Absorption of Sandwich Plates with Crushable Core", to appear in the *Proceedings of the Symposium on Recent Developments in Impact Mechanics* in honor of Professor Werner Goldsmith, UCLA, California, June 28-30, 1995.

11. Wierzbicki, T., "Crushing Analysis of Metal Honeycombs", *International Journal of Impact Engineering*, Vol. 1, No. 2, pp. 157-174.

12. Wierzbicki, T. and Hoo Fatt, M.S., "Impact Response of a String-on-Plastic Foundation", *International Journal of Impact Engineering*, Vol. 12, No. 1, 1992, pp. 21-36.

13. Hoo Fatt, M.S. and Wierzbicki, T., "Impact Damage of Long Plastic Cylinders", *International Journal of Offshore and Polar Engineering*, Vol. 2, No. 2, June 1992, pp. 147-156.

14. Jamjian, M., Sackman, J.L. and Goldsmith, W., "Response of an Infinite Plate on a Honeycomb Foundation to a Rigid Cylindrical Impactor", *International Journal of Impact Engineering*, Vol. 15, No. 3, 1994, pp. 183-200.

15. Goldsmith, W. and Sackman, J.L., "An experimental Study of Energy Absorption in Impact on Sandwich Plates", *International Journal of Impact Engineering*, Vol. 12, No. 2, 1992, pp. 241-262.

16. Cairns, D.S. and Lagace, P.A., "A Consistent Engineering Methodology for the Treatment of Impact in Composite Materials", *Journal of Reinforced Plastics and Composites*, Vol. 11, April 1992, pp. 395-412.

17. Cairns, D.S. and Lagace, P.A., "Transient Response of Graphite/Epoxy and Kevlar/Epoxy Laminates Subjected to Impact", *AAIA Journal*, Vol. 27, No. 2, November 1989, pp. 1590-1596.

18. Bernard, M.L. and Lagace, P.A., "Impact Resistance of Composite Sandwich Plates", *Journal of Reinforced Plastics and Composites*, Vol. 8, September 1989, pp. 432-445.

19. McGarry, F.J., Mandell, J.F. and Wang, S.S., "Fracture of Fiber Reinforced Composites", *Polymer Engineering and Science*, Vol. 16, No. 9, September 1976, pp. 609-614.

20. Broek, D., *Elementary Engineering Fracture Mechanics*, Kluwer Academic Publishers, Dordrecht, The Netherlands, 1986.

21. Chamis, C.C., "Simplified Composite Micromechanics for Strength, Fracture Toughness and Environmental Effects", *39th Annual Conference, Reinforced Plastics and Composites Institute, The Society of the Plastics Industry, Inc.* January 16-19, 1984.

22. Nahas, M.N., "Survey of Failure and Post-Failure Theories of Laminated Fiber-Reinforced Composites", *Journal of Composites Technology & Research*, Vol. 8, No. 4, Winter 1986, pp. 138-153.

23. Williamson, J.E., *Response Mechanisms in the Impact of Graphite/Epoxy Honeycomb Sandwich Plates*, SM Thesis, Department of Aeronautics and Astronautics, Massachusetts Institute of Technology, 1991.

24. Tsang, P.H.W., *Impact Resistance and Damage Tolerance of Composite Sandwich Panels*, PhD Thesis, Department of Aeronautics and Astronautics, Massachusetts Institute of Technology, 1994.

25. Lie, S.C., *Damage Resistance and Damage Tolerance of Thin Composite Facesheet Honeycomb Panels*, SM Thesis, Department of Aeronautics and Astronautics, Massachusetts Institute of Technology, 1989.

26. Williamson, J.E. and Lagace, P.A., "Response Mechanisms in the Impact of Graphite/Epoxy Honeycomb Sandwich Panels", *Proceedings of the American Society for Composites Eighth Technical Conference on Composite Materials*, Cleveland, OH, 1993, pp. 287-297.

27. Timoshenko, S. and Woinowsky-Krieger, S., *Theory of Plates and Shells*, McGraw-Hill Inc., 1959.

28. Szilard, R., *Theory and Analysis of Plates*, Prentice-Hall Inc., Englewood Cliffs, NJ, 1974.

29. Larsson, L. and Eliasson, R.E., *Principles of Yacht Design*, Adlar Coles Nautical, London, Great Britain, 1994.

30. Bowler, R., "Construction Design Approach for Contemporary Yacht Hulls", *The Sixth Chesapeake Sailing Yacht Symposium*, Annapolis, MD, January 15, 1983, pp. 95-101.

31. Cocquyt, A., "Advanced Materials for Yacht Construction", *9th International Symposium on Developments of Interest in Yacht Design, Yacht Building and Sailboards*, Amsterdam, Holland, March 13-14, 1986, pp. 31-68.

32. Reichard, R.P., "Structural Design and Construction of America's Cup Class Yachts", *The Tenth Chesapeake Sailing Yacht Symposium*, Annapolis, MD, February 9, 1991, pp. 17-26.

33. Curry, R., "Fiber Reinforced Plastic Sailing Yachts -- Some Aspects of Structural Design", *The Ninth Chesapeake Sailing Yacht Symposium*, Annapolis, MD, March 11, 1989, pp. 1-17.

34. Huss, J.R., *Structural Response of Marine Sandwich Panels to Uniform Pressure Loadings*, NE Thesis, Department of Ocean Engineering, Massachusetts Institute of Technology, 1990.

35. Jones, N., *Slamming Damage*, Report Number 72-4, Department of Ocean Engineering, Massachusetts Institute of Technology, May 1972.

36. Henke, D.J., *Elastic-Plastic Hull Plate Response to Slamming Induced Pressures*, MS Thesis, Department of Ocean Engineering, Massachusetts Institute of Technology, 1992.

37. Joubert, P.N., and Brown, K.C., "Pressures Generated on Hull Plating by Slamming", *Conference on Yachting Technology*, University of Western Australia, January 28-30, 1987.

APPENDIX A

1. Calculation of the A matrix for the [0/90] AS4 3501-6 graphite/epoxy laminate.

Material properties:

$E_L = 142000\ N/mm^2$

$E_T = 9800\ N/mm^2$

$G_{LT} = 7100\ N/mm^2$

Laminate 1

Angles	El (N/mm^2)	Et (N/mm^2)	G (N/mm^2)	Q11	Q12	Q16	Q21	Q22	Q26	Q16	Q26	Q66
0	1.42E+05	9.80E+03	7.10E+03	142888	2958.38	0	2958.38	9861.25	0	0	0	7100
90	1.42E+05	9.80E+03	7.10E+03	9861.25	2958.38	0	2958.38	142888	0	0	0	7100
Thickness	(mm)											
0.175		7		25005.3	517.716	0	517.716	1725.72	0	0	0	1242.5
0.175		7		1725.72	517.716	0	517.716	25005.3	0	0	0	1242.5
0.35		**14**		**26731**	**1035.4**	**0**	**1035.4**	**26731**	**0**	**0**	**0**	**2485**

Matrix A:

26731	1035.43	0
1035.43	26731	0
0	0	2485

(N/mm)

Matrix a:

3.7E-05	-1E-06	0
-1E-06	3.7E-05	0
0	0	0.0004

(mm/N)

2. Calculation of the A matrix for the [0/90] kevlar/epoxy laminate.

Material properties:

$E_L = 75000\ N/mm^2$

$E_T = 5500\ N/mm^2$

$G_{LT} = 2300\ N/mm^2$

Laminate 2

Angles	El (N/mm^2)	Et (N/mm^2)	G (N/mm^2)	Q11	Q12	Q16	Q21	Q22	Q26	Q16	Q26	Q66
0	7.50E+04	5.50E+03	2.30E+03	75641.2	1885.99	0	1885.99	5547.02	0	0	0	2300
90	7.50E+04	5.50E+03	2.30E+03	5547.02	1885.99	0	1885.99	75641.2	0	0	0	2300
Thickness (mm)												
0.175		7		13237.2	330.048	0	330.048	970.729	0	0	0	402.5
0.175		7		970.729	330.048	0	330.048	13237.2	0	0	0	402.5
0.35		**14**		**14208**	**660.1**	**0**	**660.1**	**14208**	**0**	**0**	**0**	**805**

Matrix A:

14207.9	660.096	0
660.096	14207.9	0
0	0	805

(N/mm)

Matrix a:

7.1E-05	-3E-06	0
-3E-06	7.1E-05	0
0	0	0.00124

(mm/N)

APPENDIX B

1. Calculation of the A matrix for the [0/90/0] AS4 3501-6 graphite/epoxy laminate.

Material properties:

$E_L = 142000\ N/mm^2$

$E_T = 9800\ N/mm^2$

$G_{LT} = 7100\ N/mm^2$

Laminate 3

Angles	El (N/mm2)	Et (N/mm2)	G (N/mm2)	Q11	Q12	Q16	Q21	Q22	Q26	Q16	Q26	Q66
0	1.42E+05	9.80E+03	7.10E+03	142888	2958.38	0	2958.38	9861.25	0	0	0	7100
90	1.42E+05	9.80E+03	7.10E+03	9861.25	2958.38	0	2958.38	142888	0	0	0	7100
0	1.42E+05	9.80E+03	7.10E+03	142888	2958.38	0	2958.38	9861.25	0	0	0	7100
Thickness (mm)												
0.175		7		25005.3	517.716	0	517.716	1725.72	0	0	0	1242.5
0.175		7		1725.72	517.716	0	517.716	25005.3	0	0	0	1242.5
0.175		7		25005.3	517.716	0	517.716	1725.72	0	0	0	1242.5
0.525		**21**		**51736**	**1553.1**	**0**	**1553.1**	**28457**	**0**	**0**	**0**	**3727.5**

Matrix A:

51736.3	1553.15	0	
1553.15	28456.8	0	(N/mm)
0	0	3727.5	

Matrix a:

1.9E-05	-1E-06	0	
-1E-06	3.5E-05	0	(mm/N)
0	0	0.00027	

2. Calculation of the A matrix for the [0/90/0/90] AS4 3501-6 graphite/epoxy laminate.

Material properties:

$E_L = 75000\ N/mm^2$

$E_T = 5500\ N/mm^2$

$G_{LT} = 2300\ N/mm^2$

Laminate 4

Angles	El (N/mm^2)	Et (N/mm^2)	G (N/mm^2)	Q11	Q12	Q16	Q21	Q22	Q26	Q16	Q26	Q66
0	1.42E+05	9.80E+03	6.00E+03	142888	2958.38	0	2958.38	9861.25	0	0	0	7100
90	1.42E+05	9.80E+03	6.00E+03	9861.25	2958.38	0	2958.38	142888	0	0	0	7100
0	1.42E+05	9.80E+03	6.00E+03	142888	2958.38	0	2958.38	9861.25	0	0	0	7100
90	1.42E+05	9.80E+03	6.00E+03	9861.25	2958.38	0	2958.38	142888	0	0	0	7100
Thickness (mm)												
0.175		7		25005.3	517.716	0	517.716	1725.72	0	0	0	1242.5
0.175		7		1725.72	517.716	0	517.716	25005.3	0	0	0	1242.5
0.175		7		25005.3	517.716	0	517.716	1725.72	0	0	0	1242.5
0.175		7		1725.72	517.716	0	517.716	25005.3	0	0	0	1242.5
0.7		**28**		**53462**	**2070.9**	**0**	**2070.9**	**53462**	**0**	**0**	**0**	**4970**

Matrix A:

53462.1	2070.86	0	
2070.86	53462.1	0	(N/mm)
0	0	4970	

Matrix a:

1.9E-05	-7E-07	0	
-7E-07	1.9E-05	0	(mm/N)
0	0	0.0002	